UCLouvain

École polytechnique de Louvain

Design, fabrication and testing of wideband grounded coplanar waveguide (GCPW) to substrate-integrated waveguide (SIW) transitions for W band circuits

Author: **Adam Abazi**
Supervisors: **Dimitri Lederer, Jean-Pierre Raskin**
Readers: **Isabelle Huynen, Vincent Kaschten**
Academic year 2021–2022
Master [120] in Electrical Engineering

Acknowledgments

I would like to thank the valuable people who helped and supported me throughout this master's thesis and without whom its completion would not have been possible.

First of all, I want to thank my supervisors, Prof. Dimitri Lederer and Prof. Jean-Pierre Raskin. They were always available when I needed them whether it was for advances or failures.

I would also like to thank Martin Rack and Lucas Nyssens for their precious help.

In particular, I would like to thank Lucas Nyssens for his help with everything related to measurements and calibration. I will never be able to repay him for the time he spent on my behalf.

I would like to thank Isabelle Huynen and Vincent Kaschten for taking time to read this thesis.

Finally, I would like to thank my family and relatives not only for their support during this work but also for their support throughout my studies.

Abstract

Substrate-integrated waveguide is a promising technology for RF integrated and high-frequency circuits. But to measure them and interconnect them with other transmission line technologies, transitions are necessary.
The purpose of this master's thesis is to design, fabricate and measure wideband transitions between grounded coplanar waveguides (GCPW) and substrate-integrated waveguides (SIW) for the W band. The substrate used is a BenzoCycloButene polymer (BCB).

Contents

Chapter 1

Introduction

Since its introduction by Ke Wu and Dominic Deslandes in 2001 in [1], substrate integrated waveguide technology (SIW) has attracted a lot of interest in the RF research community. Before that, conventional waveguides were too massive and required complex structures to be connected to integrated circuits. Now, rectangular waveguides can be fabricated and integrated in planar substrates using existing microfabrication or PCB techniques.

This technological advancement is particularly interesting in the context of high-frequency circuits since it allows for low-loss RF circuits that are isolated from the noise of other electrical components.
For this purpose, the use of BenzoCycloButen (BCB) as a substrate for high-frequency SIW applications has been proposed in [2].

To take full advantage of SIW technology, it is necessary to create efficient transitions. Indeed, one purpose of having waveguides integrated into the substrate is to be able to connect it to other transmission line technologies.
Moreover, to measure circuits made of SIW, it is necessary to feed them with other technologies. One of the most common planar transmission line technologies used when performing measurements on RF circuits is the grounded coplanar waveguide (GCPW).

In this context, it is clear that transitions between GCPWs and SIWs for high-frequency circuits are of great use.

In chapter 2, an overview of transitions between any feeding technology and SIW will be made. In addition to that, it will also introduce briefly the main transmission line technologies. Then, in Chapter 3, transitions between GCPWs and SIWs will be designed using BCB substrate-integrated waveguide technology for the W band. This chapter will also make a detailed explanation of the steps leading to the final design.
As the objective of the SIW circuits is to be used in real applications, a description of how to manufacture the designed transitions, in order to be able to measure them afterwards, will be made in chapter 4.
Finally, in chapter 5, performances of tests that will be made on the fabricated transitions will be presented.

Chapter 2

State of the art

In order to understand the utility of a transition from a grounded coplanar waveguide (GCPW) to a substrate-integrated waveguide (SIW) in the W band, a survey of the state of the art of transitions between any feeding technology and a SIW is necessary. In addition to that, a word is given on the most widely used transmission lines for transitions in order to have the theoretical background for the technologies covered in this work.

2.1 Transmission lines technologies

For this chapter, and more generally, for this work, three transmission lines will be mainly used, namely the microstrip line, the grounded coplanar waveguide (GCPW) and the substrate-integrated waveguide (SIW). The coplanar waveguide technology (CPW) will also be discussed rapidly as it presents similarities with the grounded coplanar waveguide and to emphasize why it is better and easier to use GCPW.

2.1.1 Substrate-integrated waveguide

The substrate-integrated waveguide is a technology that was introduced within the past 20 years. It is a technology that has attracted a lot of interest in recent years because it offers a perfect compromise between a high-quality factor technology, namely the rectangular waveguide, and an easy-to-integrate planar line [1]. Moreover, compared with the other planar technologies, the SIW has the advantage of lower loss, higher power handling capability and good isolation with adjacent SIW [3]. However, integrating the waveguide in the substrate decreases the quality factor but it remains higher than for the other planar transmission lines technologies.
The first time SIW appeared in an article was in [1] and two ways to integrate the waveguide in the substrate were proposed.
The first is to use periodic via holes so that the fields act with these rows as if they were walls. In order for this technique to work, some design rules have been developed in [4] and detailed in [2]. These are the following:

$$\begin{aligned} p &> D \\ p/\lambda_c &< 0.25 \\ p &\leq 2D \end{aligned}$$

with p the pitch width (distance between two via hole centers), D the via hole diameter and λ_c the cut-off frequency of the first waveguide mode (TE_{10}). This technique is the most widely used because of its compatibility with traditional PCB technology.
The second one is to use full metallic sidewalls named metalized grooves. This technique removes the additional constraint due to the vias but is harder to integrate which makes it a less-used technique.
Both techniques can be seen in figure 2.1.

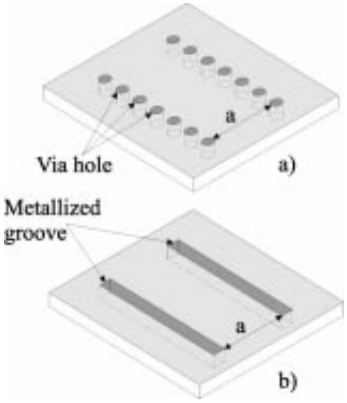

Figure 2.1: Techniques to integrate a waveguide in a substrate from [1]. a) rows of via holes technique b) metalized grooves technique

In addition to these two main techniques, [3] introduces two other types of vias for terahertz applications. These vias have not longer a circular section but are oval shaped and they can be transverse or longitudinal oriented.

2.1.2 Microstrip line

Microstrip line technology is one of the most widely used planar transmission lines. This is due to its simplicity of fabrication and design as well as its ability to be easily miniaturized. In the context of transitions to an SIW, microstrip line is well suited to match the first mode of the SIW (TE_{10} mode) because its fields are quasi-TEM if the substrate can be considered thin enough that is, when $d << \lambda$ with d the substrate thickness and λ the wavelength associated to the microstrip. Figure 2.2 shows the geometry and the field lines associated to the microstrip line.

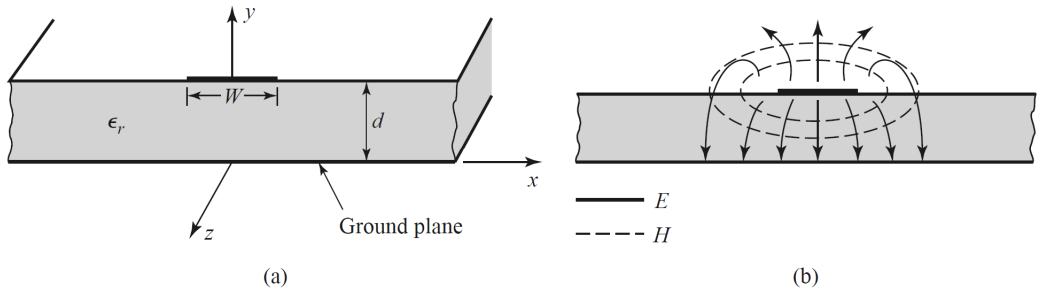

Figure 2.2: Microstrip line from [5]. a) Geometry of the line b) Electric (E) and magnetic (H) field lines

The microstrip line is a technology that is well-established and therefore, equations to know its characteristics are defined. However, in order to describe them, an approximation has to be made that is, one can consider the microstrip line as being a strip of metal in a constant dielectric medium at a distance d of the ground plane (corresponding to the substrate thickness) under the condition that the dielectric constant, or relative permittivity, of the substrate is replaced by an effective one which takes the air and the substrate into account. The relation is the following [5]:

$$\epsilon_e = \frac{\epsilon_r + 1}{2} + \frac{\epsilon_r - 1}{2} \frac{1}{\sqrt{1 + 12d/W}} \tag{2.1}$$

with ϵ_e the effective permittivity, ϵ_r the relative permittivity, d the substrate thickness and W the metallic strip width.
This approximation allows to establish two relations, one that gives the characteristic impedance knowing the dimensions of the strip and one that gives the ratio between the width and the thickness knowing the characteristics impedance of the line. They can be found in [5]. However, the efficiency of microstrip lines must be qualified because they suffer from more radiation losses and are more dispersive than other transmission lines [6].

2.1.3 Coplanar waveguide

Before introducing the grounded coplanar waveguide, which is the transmission line used for the transition to substrate-integrated waveguide used in this work, an introduction to the coplanar waveguide is useful to understand the advantages of the former.
The coplanar waveguide (CPW) is a planar transmission line in which the grounds are brought to the upper plane on both sides of the central strip. As for the microstrip line, the central strip carries the signal. The structure then forms what is named a ground-signal-ground (GSG). The coplanar waveguide presents several advantages among which: an easy fabrication, the absence of via holes or wraparound, less radiation loss and the support of even or odd quasi-TEM modes [7] [5]. Moreover, measurement techniques have been developed especially to carry-out the GSG configuration. However, these techniques involve more conductor losses than for the microstrip measurements. Figure 2.3 shows representations of a coplanar waveguide and its fields profile.

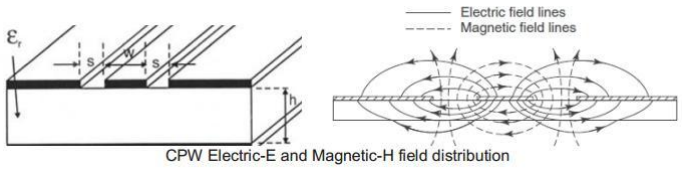

Figure 2.3: Coplanar waveguide structure and its field profile from [8]

2.1.4 Grounded coplanar waveguide

The grounded coplanar waveguide, also named conductor-backed coplanar waveguide, is a transmission line technology that offers a perfect trade-off between the microstrip line and the coplanar waveguide. The grounded coplanar waveguide consists of a coplanar waveguide with a ground plane added below the ground-signal-ground plane which is connected to the ground of the upper plane thanks to metalized vias holes or metalized sidewalls. This configuration then provides kind of a mix between the microstrip line and the CPW fields profile [6].

The GCPW has the same advantage than the CPW line in terms of radiation loss and it is even more advantageous for the GCPW as more field lines are in the substrate [7] but also suffers from the measurement loss problem [6]. Moreover, the GCPW is less dispersive and is more robust against crosstalk than microstrip and CPW [6]. Furthermore, GCPW is good at reducing the parasitic wave mode propagation.
All of the above-mentioned qualities of GCPW makes it a well-suited technology for high-frequency applications and for transitions to substrate-integrated waveguides. However, it is important to note that the theoretical framework for the study of GCPWs is limited to the case of substrates of fairly large thickness and to not too large frequencies. The established equations for this case can be found in [7]. For the other cases, a full-wave simulation design is necessary.
Figure 2.4 represents the fields profile of a grounded coplanar waveguide without considering the metalized via holes walls or the metalized sidewalls but the profiles are very similar with and without them.

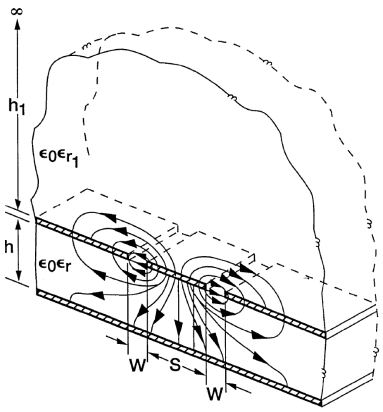

Figure 2.4: Fields profile of a grounded coplanar waveguide from [7]

2.2 Microstrip to SIW

Microstrip to SIW transitions are the most commonly used transition when it comes to using SIW. In fact, they are at the origin of the creation of the SIW principle. Indeed, the article "Integrated Microstrip and Rectangular Waveguide in Planar Form" [1] aimed to propose, as the title suggests, a transition between a microstrip and a rectangular waveguide in a planar form. Doing this, the autors created the first-ever Substrate-Integrated Waveguide. This shows the importance and usefulness of this kind of transitions. The following of this section describes the most widely used and innovative microstrip to SIW transitions.

2.2.1 Tapered transition

Principle

The principle of this kind of transitions is pretty simple. It makes use of the field lines similarities between the microstrip lines and the SIW. Indeed, as it can be seen on the figure 2.5, the dominant mode of the electric field of the microstrip line and the SIW are similar to each others, they share the same profile [1].

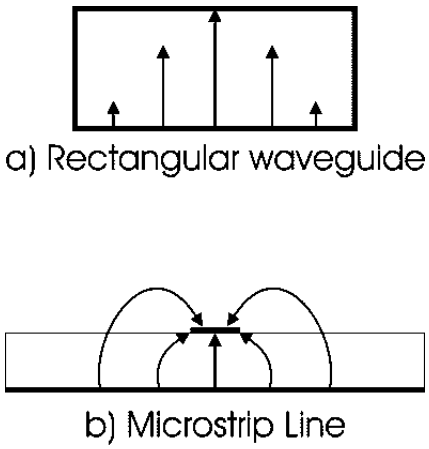

Figure 2.5: Dominant electric mode field lines for the SIW (a) and the microstrip line (b) from [1]

The transition then consists in widening the microstrip line in order to align more and more the electric field lines. This is done by using a tapered microstrip section. The transition design can be seen in figure 2.6.

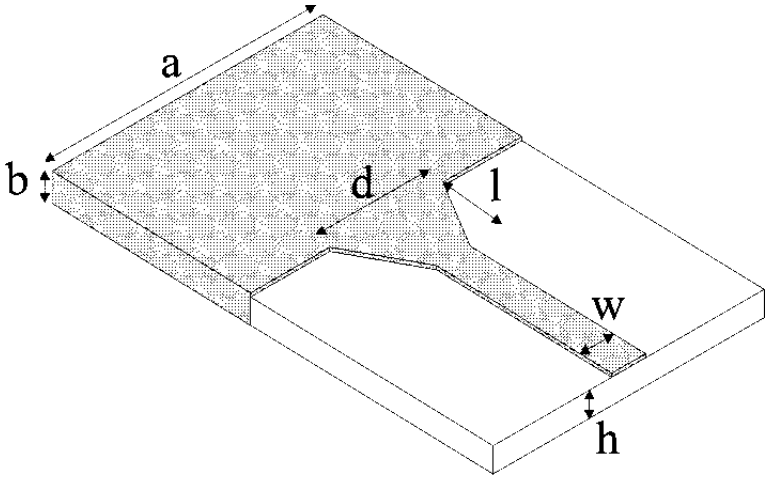

Figure 2.6: Microstrip to SIW transition from [1]

This structure is convenient because of its simplicity, ease of design and relatively good performances.

Technical specifications and implementation

For tapered microstrip to SIW transitions, design equations have been established in [9]. These equations give the microstrip width in order to get the best impedance to ease the field matching as well as the width and the length of the taper to obtain the best matching - the lowest return losses. However, these equations are approximations. Moreover, the nature and properties of the substrate affect the design parameters significantly [9] - a smaller substrate tends to increase losses in the microstrip line as well as in the SIW, thus reducing the performances of the transition [1]. Therefore, most of the tapered microstrip to SIW transitions have been designed using full-wave simulations and by optimising the design parameters (line width,

taper width and taper length). To do it, a full design is made and simulated using a full-wave simulator, as CST or HFSS. The simulated transitions are then optimized by iteration [1].

Performances and results

The transition designed in [1] has the following design parameters (results are given for a back-to-back configuration $16mm$ long): dielectric substrate with a thickness of $0.254mm$ and a relative permittivity of $\epsilon_r = 2.33$, a microstrip line width of $0.711mm$, a taper width of $2.286mm$ and a taper length of $5.588mm$. The SIW is designed for the LMDS ($28 - 31GHz$ [10]) frequency range. Results for this transition are the following: a bandwidth from 26.65 to $30.20GHz$ with $20dB$ return loss and insertion loss better than $0.3dB$ and the entire band. These results can be seen in figure 2.7. This figure is also used to demonstrate how to represent return and insertion losses.
Using different configurations, authors of [9] have achieved the following results:

1. return loss better than $20dB$ from 18 to $26.5GHz$ for an alumina transition of thickness $0.254mm$ and relative permittivity of 9.9;

2. return loss better than $20dB$ from 50 to $75GHz$ for an alumina transition of thickness $150\mu m$ and relative permittivity of 3.15;

3. return loss better than $18dB$ from 24 to $38GHz$ for an alumina transition of thickness $150\mu m$ and relative permittivity of 3.15;

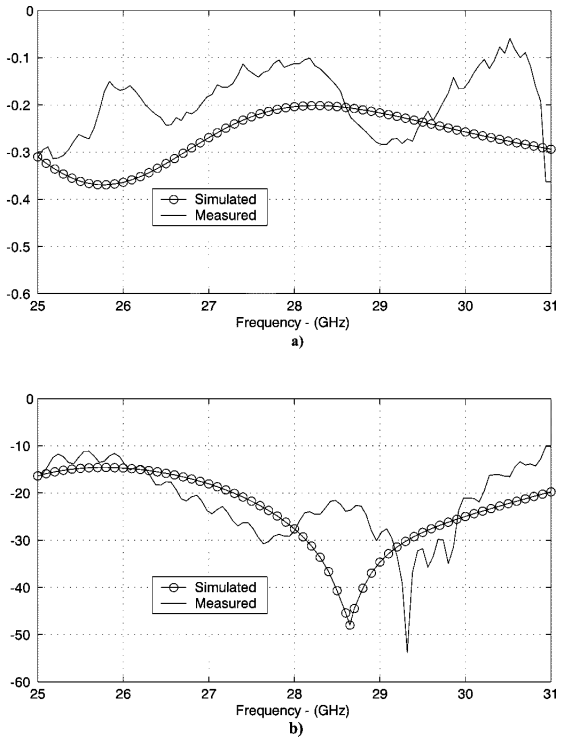

Figure 2.7: Results for taper microstrip to SIW transitions in a back-to-back configuration from [1]. a) insertion loss; b) return loss

Variants of tapered transition

Since the first tapered microstrip to SIW transition was proposed in 2001 by Deslandes D. and Wu K., other transitions improving the taper principle have been proposed. Firstly, a transition with a slight difference has been proposed in [11] called *taper-via transition*. The modification consists of tapering not only the microstrip line but also the SIW. To do so, 2 vias are added between the end of the microstrip taper section and the beginning of the SIW section. Moreover, they are placed toward the inside such that they are staggered with respect to the SIW vias rows as shown in figure 2.8.
This configuration allows for a better matching due to a more confined field in the lateral direction.

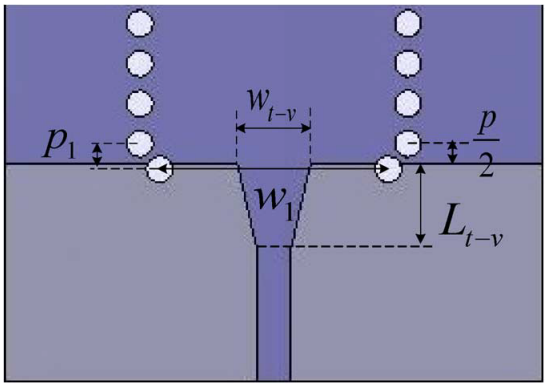

Figure 2.8: Structure of the tapered via transition from [11]

Using these taper-via transitions, the authors of the article [11] have been able to design microstrip to SIW transitions in multiple bands (X, Ku, K, Ka, U and E) which are about $10dB$ better in average in terms of return loss.

Secondly, a transition using ESIW (SIW filled with air, empty) has been proposed in [12] which consists of two tapers facing each others. The first one is made in microstrip technology and the other one is in the air part of the ESIW. The whole structure can be seen in figure 2.9. This kind of transitions provides results that are better on average for the whole frequency band considered than classic tapered transitions from microstrip to ESIW but it suffers from performances loss around the central frequency. It achieves $20dB$ return loss and $0.6dB$ insertion loss over the full bandwith (for the band corresponding to WR-28 SIW) against $13.5dB$ return loss and $0.6dB$ insertion loss for the conventional taper.

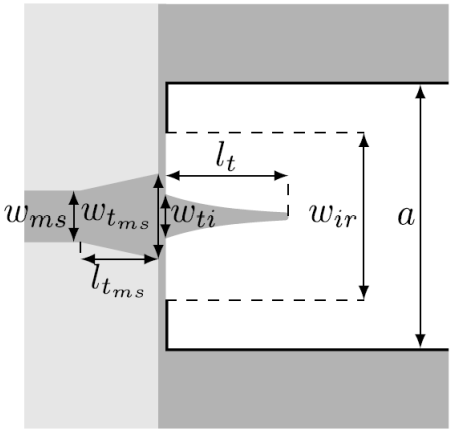

Figure 2.9: Structure of microstrip to ESIW transition from [12]. Light grey is the substrate, white is air and dark grey is metal.

Thirdly, a transition using multiple tapers in cascade is designed in [13]. The idea here is to use multiple tapers in order to adapt the impedance to match a specific frequency and a narrow band. The designs have been done to optimise the frequency range from 24.25 to $27.5GHz$ and the results are the following: return loss of $35dB$ minimum and insertion loss of $1.05dB$ maximum.

2.2.2 Lumped microstrip to SIW transition

Principle

Another kind of transition was proposed in [14] with a completely different paradigm. Instead of considering a transition based on the field matching (mode matching) in a geometric way, the transition here uses lumped elements in order to modify the imaginary part of the impedance. As a reminder, the impedance of any electrical element can be written in a complex form as:

$$Z = R \pm jX$$

where Z is the impedance, R is the real part of this impedance corresponding to a purely resistive element and X is the imaginary part corresponding to a capacitive (minus sign) or a inductive (plus sign) element. The working principle of the transition is then to add capacitance and inductance as lumped elements in order to compensate for the imaginary part of the impedance and to try to bring the real part to a 50Ω value. Two configurations are proposed and these are shown in figure 2.10. The first one uses series inductance and shunt capacitance offering a low-pass matching and the other one uses series capacitance and shunt inductance providing a high-pass matching. Both of them are convenient to achieve impedance and mode matching but a phase shifting is introduced, respectively forwards and backwards.

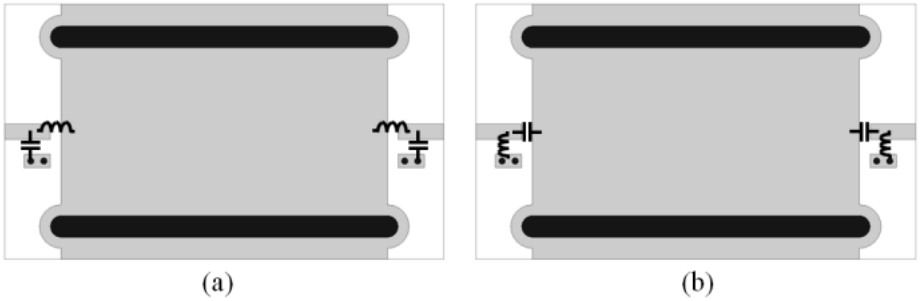

Figure 2.10: Microstrip to SIW transition using lumped elements from [14]. a) series inductance and parallel capacitance; b) series capacitance and parallel inductance

Advantage and drawback of lumped transition

The main advantage of lumped transitions is its small length. Indeed, since it does not need to do a geometric match, the transition takes almost no place at all. This allows an easier integration in low frequency ranges. However, using lumped element only works when they are easy to integrate which is not the case for high frequency applications.

Performances and results

In [14], two transitions were simulated and measured. One using a low-pass matching and the other one using a high-pass matching. Both provides similar results which are: a frequency range of 4.04 to $5.67GHz$ with return loss better than $10dB$ and insertion loss better than $1.3dB$ for the first one and a frequency range of 3.9 to $5.12GHz$ with return loss better than $10dB$ and insertion loss better than $1.3dB$ for the second one.

2.3 Coplanar waveguide (CPW) to SIW

Coplanar waveguide (CPW) to SIW as well as the next investigated kind of transitions, Grounded coplanar waveguide (GCPW) to SIW, are really pertinent. Indeed, the CPW and the GCPW technologies are widely used to design and to measure circuits at high frequencies. Consequently, they are also used a lot to measure circuits with a ground-signal-ground (GSG) probe and this helps to justify the utility of these kind of transitions.
This section aims to present the CPW to SIW transitions while the next one will present the GCPW to SIW ones.
The distinction is made to avoid confusion.

There are not many transitions that use the classic CPW technology. This is due to the principle of substrate-integrated waveguide which requires metal on the upper and on the lower plane of the structure. Indeed, having metal on the back of the whole structure is easier, especially in the high frequency ranges where the dimensions are in the order of tens or hundreds of microns, than keeping metal only on a specific part only. Nevertheless, three of them can be found in the literature.

2.3.1 90° bent slots CPW to SIW transition

The first proposed CPW to SIW transition is the one from [15].

Principle

The design principle of this transition is to have a coplanar waveguide with both slots terminated by a $90°$ bend $\lambda/4$ long in short-circuit ending. In addition to that, two stubs are added in the CPW line to match the transition as well as two vias to remove any parallel mode that could propagate [15]. In terms of physics principle, the transition matches the fields from the CPW to the one from the SIW by transforming the field lines due to the bends and the short circuit ending. Indeed, the field in this configuration are minimum on the end of the slot and maximum on the center as it is the case for the first mode of the SIW.
The structure in a back-to-back configuration is represented in figure 2.11.

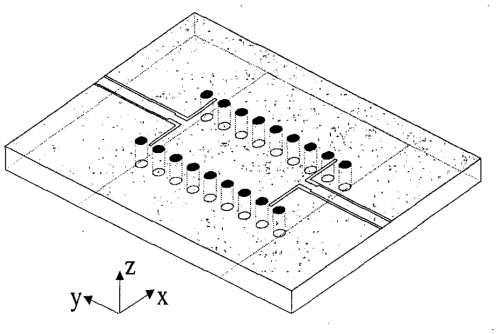

Figure 2.11: Back-to-back configuration of 90° bent slots CPW to SIW transitions from [15]

Parameters and results

In [15], the transition is designed to work in the LMDS frequency range on a substrate with a height of $0.508mm$ and a relative permittivity of 2.33. The SIW section is $10mm$ long and the transition parameters have been optimized using finite element method package. The optimized performances of this design are the following: a 7% bandwidth(from 27.5 to $29.5GHz$) with $15dB$ return loss and measured insertion loss better than $3.2dB$.

GCPW to SIW equivalent

In [16], an equivalent to this transition is presented in the case where the feeding line is a grounded coplanar waveguide instead of a coplanar waveguide. There is no fundamental difference in the principle of operation and therefore, a whole section for this case is not justified. The performances of the transition in this case, using a $381\mu m$ with a relative permittivity of 9.7 (Alumina) are: return loss lower than $15dB$ and insertion loss better than $1.2dB$ between 39 and $59GHz$.

2.3.2 Taper-in CPW to SIW transition

Another transition from CPW to SIW was designed in [17].

Principle

The idea here is to use the two metallization planes in order to design a transition which presents a taper-in on the CPW plane. The configuration is represented in figure 2.12. Once

again, the principle is to transform the field lines so that the field that is mostly concentrated in the slot end up having the same profile as the one of the first propagating mode of the SIW.

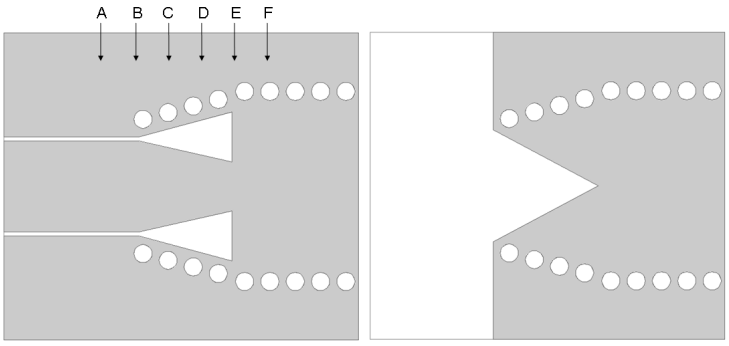

(a) Front metallization (b) Back metallization

Figure 2.12: Front and back metallization of the transition from [17]

Parameters and results

The transition in [17] is designed to work in the 18 to $28GHz$ frequency range, on a RT/Duroid 6002 substrate with a thickness of $0.508mm$ and a relative permittivity of 2.94. The CPW line is designed to be 50Ω and the transition parameters are optimized using a full-wave simulation package. The performances obtained with this configuration are the following: return loss better than $17dB$ and insertion loss better than $1.45dB$ over the full bandwidth.

2.3.3 CPW to SIW transition using elevated coplanar waveguide (ECPW)

The third transition from classic CPW to SIW is the one from [18]. It uses an elevated coplanar waguide section which is an intermediate section made of a metalized via hole.

Principle

The transition presented here is somewhat different from those before in that it involves 3 layers. Indeed, the working principle is to transform the field profile of the CPW by using an elevated coplanar waveguide (ECPW) as an intermediate section to do the transition. The structure is therefore more complicated to fabricate since it requires an additional layer of metal. The structure is represented in figure 2.13. The field profiles along the transition is also shown in the figure as it allows to understand the fields transformation in a generic way.

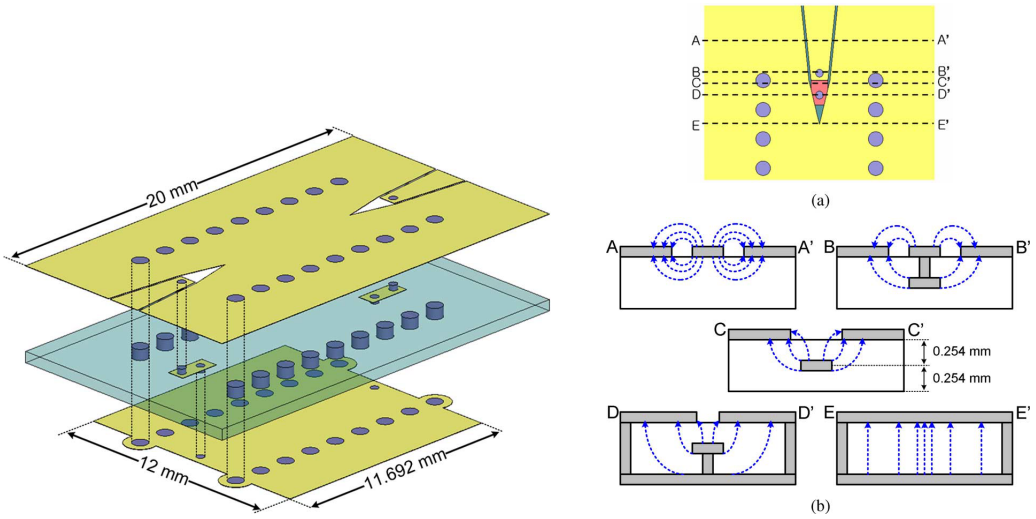

(a) Transition structure (b) Field profiles along the transition

Figure 2.13: Structure of the transition and field profiles from [18]

Parameters and results

The transition in [18] is designed to work in the 19 to $40GHz$ frequency range on a Taconic dielectric substrate with a thickness of $0.254mm$ and a relative permittivity of 2.33. The CPW line and the transition parameters are optimized using HFSS, a 3-D FEM simulator. The performances obtained with this configuration are the following: return loss better than $10dB$ and insertion loss better than $2dB$ over the full bandwidth.

2.4 Grounded coplanar waveguide (GCPW) to SIW

As mentioned in the previous section, GCPW to SIW transitions are widely used. This is due to the advantages that can be exploited from GCPW lines such as the simplicity of design of such a line and the proximity of the field profile (quasi-TEM planar mode) to that of SIW lines. Among the many designs of transitions between coplanar and substrate-integrated waveguides, the most varied of them are presented here along with variants of the same principles.

2.4.1 Taper GCPW to SIW transitions

In [19] and [2], the same geometric configuration of GCPW to SIW transition have been proposed but with different substrates and working frequencies.

Principle

As in section 2.2.1, the design idea of the transition here is to use a taper in order to transform the field profile of the line to the one of the SIW. To do this, the slot is widened to make room for the metalized taper. The vias walls are also tapered.
This is represented in figure 2.14.
As with the tapered microstrip to SIW transition, the goal is to transform the GCPW line fields to have the same shape as the first mode of the integrated waveguide. In addition, the transition also acts as an impedance transformer [20], which then provides a good matching. In order to

get the right matching, three parameters are tuned: the taper angle of the slot, the taper angle of the center metal and the transition length.

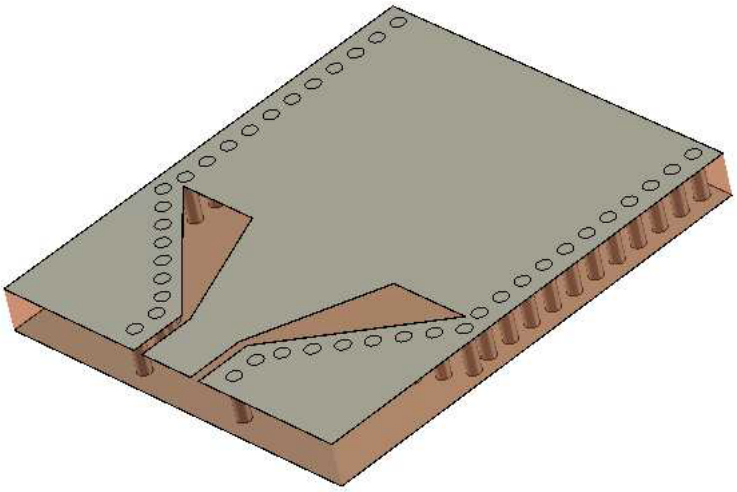

Figure 2.14: GCPW to SIW tapered transition from [19]

Parameters and results

For the transition designed in [19], the following constraint parameters were used: substrate of $1.524mm$ thickness with a relative permittivity of 3.38 (RO4003c). The performances obtained with this configuration and the optimised parameters are: return loss better than $10dB$ over a frequency range from 7 to $14GHz$ and insertion loss better than $0.5dB$ for the same band.

For the transition design in [2], the following constraint parameters were used: substrate of $30\mu m$ thickness with a relative permittivity 2.68 and 2.5, decreasing with increasing frequency (BCB - CYCLOTENE 3022-63) and the frequency range targeted is the W band. The performances obtained with this configuration and after optimization of the design parameters are: return loss better than $15dB$ over a frequency range from 77 to $106GHz$ and insertion loss better than $4dB$ for the same band.

Precision on [2]

As for this work, the transition presented in [2] uses BCB substrate-integrated waveguides at high frequencies. The technology will be detailed further but a few words can be given here to emphasize the differences with the others transitions presented.
The BCB substrate-integrated waveguides are slightly different than other SIW. They are integrated in a BCB substrate which is deposit on top of a metal layer itself deposited on a Silicon layer. According to [2] this substrate allows for a better handling of the high frequencies.

Variants of the tapered GCPW to SIW transitions

In [21], another kind of tapered transition is proposed. The differences with the one described above are that the slot of the GCPW is not widened and the via walls are not tapered. However, the physical principle works the same way as before. The simplicity of design as well as the good performances it achieves makes it a good trade-off. The structure is represented in figure

2.15. The impedance and mode matching are done using two main parameters, namely the taper length and the paper angle, the first one being more influential than the second one. The performances of this transition realised over a $0,508mm$ substrate with relative permittivity of 2.94 (Rogers RT/duroid 6002) are, for a targeted Ka band (26.5 to $40GHz$): return loss better than $20dB$ and insertion loss better than $0.4dB$ over the full bandwidth.

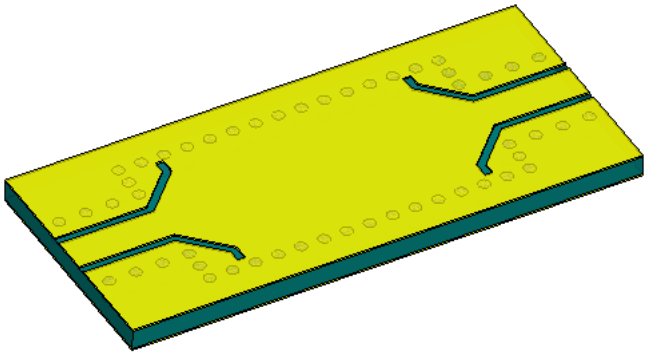

Figure 2.15: Alternative tapered GCPW to SIW transition from [21]

Another transition is proposed in [14]. As for the tapered microstrip to SIW transition, it uses multiple tapers in cascade is proposed for a GCPW feeding line. Here again, the bandwidth is pretty narrow so it is not developed any further in this work.

2.4.2 Current probe GCPW to SIW transition

A transition with a completely different design idea is proposed in [22].

Principle

The operating principle of this transition is to use a current probe in order to excite the SIW first mode. The current flows through the GCPW and then gets in the probing via, creating a magnetic field which matches the SIW first mode magnetic field [22]. This is similar to the idea used for classic rectangular waveguides. In addition to this probe, an open-circuit has to terminate the line. The transition is shown in figure 2.16.

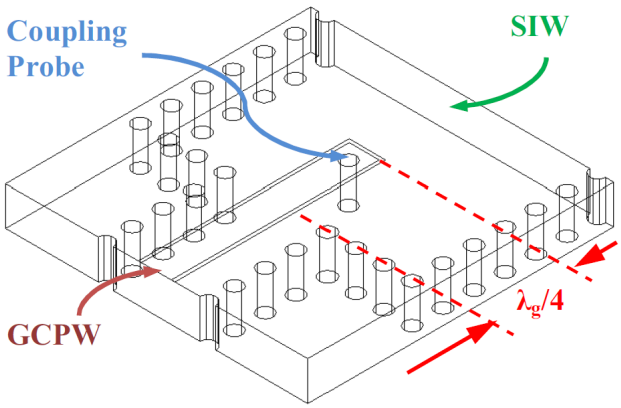

Figure 2.16: Current probe GCPW to SIW transition from [19]

Parameters and results

The performances obtained for this transition realised over a $0.762mm$ substrate with a relative permittivity of 2.94 and optimized for the central frequency $28GHz$ are the following: a higher than $20dB$ insertion loss over a narrow frenquency range from 26.96 to $29.8GHz$ and insertion loss smaller than $0.73dB$ over the same band.

2.5 Other transitions

For the sake of completeness, mention is made of transitions between non-planar feeding technologies and substrate-integrated waveguides, without going into too much detail, in the following of this section.

In [23] and [24], transitions between classic rectangular waveguides and substrate-integrated waveguides are proposed. The first one consists of a complex three-dimensional structure using 3 substrates layers with vias and slots in a specific shape. This transition targets the V band and achieves return loss higher than $10dB$ while insertion loss is lower than $0.48dB$ over the full bandwidth on a substrate with two different heights ($0.787mm$ and $0.508mm$) and a relative permittivity of 2.24 (Rogers 5880).
The second one has a simpler geometry. It consists of a fin line deposited on the same substrate as the SIW one. For a targeted range frequency corresponding to the Ka band, return loss better than $15dB$ and insertion loss less than $1.4dB$ are achieved over the full band on a $0254mm$ thick substrate with a relative permittivity of 2.22 (RT/Duroid 5880).
Both transitions are shown in figure 2.17.

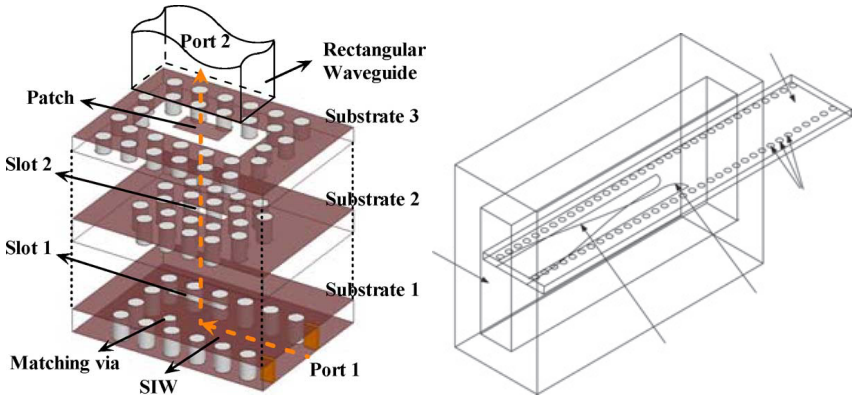

(a) 3D rectangular waveguide to SIW transition

(b) Planar rectangular waveguide to SIW transition

Figure 2.17: Waveguide to SIW transitions a) from [23] b) from [24]

In [25], a transition that interconnects a coaxial cable and a substrate-integrated waveguide is proposed. The structure is similar to what is done for planar technologies except that, here, a coaxial cable will be plugged into the transition. The working principle of the transition is to use a taper with a probe in the form of a via in the taper center which excites the TE_{10} mode of the SIW and is connected to the coaxial cable. Using a $0.787mm$ thick substrate with a relative permittivity of 2.2 (RT Duroid 5880), the transition, designed to operate at X band (8 to $12GHz$), presents insertion loss better than $1.2dB$ and return loss better than $15dB$ for a 30% bandwidth. The structure is represented in figure 2.18

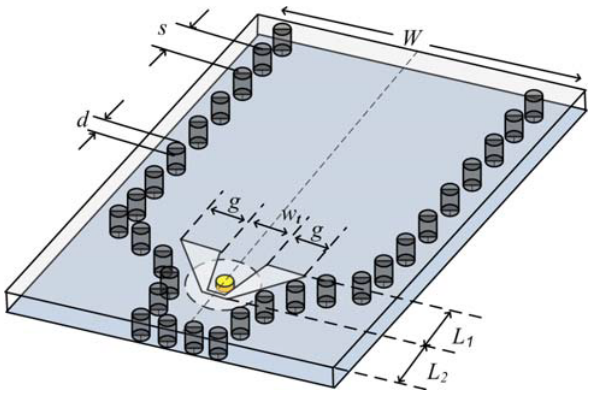

Figure 2.18: Coaxial to SIW transition from [25]

The last transition worth mentioning is the one from [26]. It is a transition between a stripline and a substrate-integrated waveguide. A stripline is a non-planar transmission line consisting of a metal strip inserted in a substrate with ground planes below and above. The transition uses once again the taper principle but in order to realize a strip line, a second substrate layer with metal deposited in a specific shape is added above. Using a $0.508mm$ thick substrate with a relative permittivity of 2.94 (RT/Duroid 6002), the transition presents insertion loss better than $0.44dB$ and return loss better than $24dB$ for a frequency range from 18 to $28GHz$. The structure of the transition is represented in figure 2.19 in exploded view.

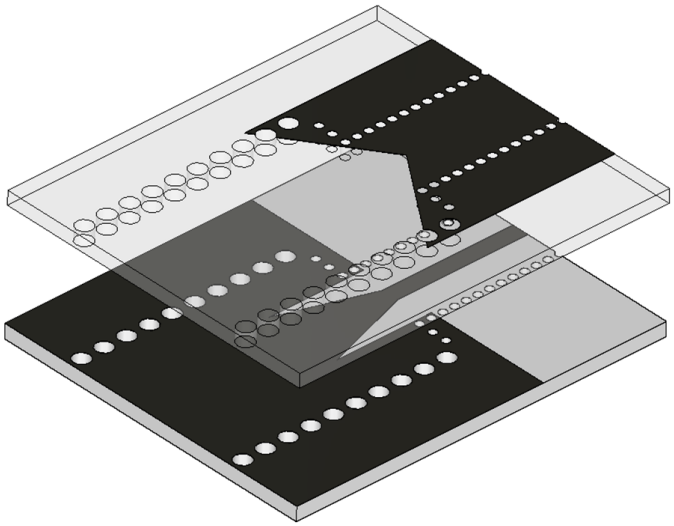

Figure 2.19: Stripline to SIW transition from [26]

Chapter 3

Design

From the study of the state of the art, a need for transitions between a planar transmission line technology and a substrate-integrated waveguide for high frequencies has emerged. This is especially true in the W band where only one design has been proposed in [2]. It is also apparent that transitions with a small substrate thickness are rare.
This chapter describes the design path for new transitions between a grounded coplanar waveguide and a substrate-integrated waveguide to address these needs. This is done by first laying the groundwork that will guide and constrain the designs such as substrate constraints and line dimensions. An important discussion on the full-wave simulation tool used for the design will also be made. Then, a first transition test based on what is done in the literature will be described. This will be the starting point for the development of original transitions that aim to address the problems encountered by the usual transitions in such a context. For the final transition designs, the conductor losses will be added to the simulation.
In a final step, simulations will be performed considering a problem highlighted in the simulation tool discussion.

3.1 Preliminaries

The following describes the constraints due to the manufacturing process as well as the designs of the GCPW and SIW lines, invariable for the rest. In addition to that, the discussion about CST Studio Suite 2021 as a full-wave simulation tool is made here in order to understand the following of the process.

3.1.1 Fabrication process constraints

The manufacturing process will be described briefly in chapter 4 but it is already necessary to define the parameters that are linked to it and that constrain the design. Indeed, to start the design, it is necessary to choose the exact technology that will be used. The choice was made here on the basis of Nicolas Vanpée's work in the framework of his master's thesis, which develops a fabrication process of substrate-integrated waveguide using a BCB substrate. To be precise, the substrate used is the CYCLOTENE 3000 series BCB which is a non-photosensitive benzocyclobutene resin [27]. This BCB was developed to be used as a dielectric.
This choice introduces the following constraints:

1. the substrate thickness is $16.5\mu m$

2. the dielectric constant (relative permittivity) is $\epsilon_r = 2.5$

Even though the dielectric constant may change with the frequency, for simplicity it will be assumed constant.
In addition to that, the metal used is a $0.5\mu m$ thick aluminum. This metal has the advantage of being easy to deposit and its properties allow to consider a perfect conductor in a first instance of the design process without losing too much generality.
The last manufacturing design constraint is about the choice between metalized via holes or metalized sidewalls. The process developed here makes it easy to use metalized sidewalls and thus, it is the technique that will be used. As it was pointed out in the study of the state of the art, the use of sidewalls removes the difficulty of designing vias for them to act like walls.

3.1.2 SIW line design

The first step in the design process is to set up the substrate-integrated waveguide that will be used for the rest of the work.
As the manufacturing constraints detailed in section 3.1.1 indicate, the SIW is designed with full metalized sidewalls. This is the configuration mentioned in section 2.1.1 that was first introduced in [1].
This configuration facilitates the design of the SIW because it can then be considered as a classical rectangular waveguide filled with a dielectric. Therefore, the usual waveguide theory can be used to dimension the SIW [28].

Dimensioning

To size the SIW, the dimensions of the section must be determined. By convention, in the following, a will correspond to the length of the biggest side and b will correspond to the length of the smallest side as it is illustrated in figure 3.1.
The smaller side width is determined by the substrate thickness since the waveguide is integrated in the substrate, thus $b = 16.5\mu m$.
To determine a, it is necessary to use waveguide equations. The only mode that must propagate in the waveguide is the TE_{10} mode as it is the first and dominant mode. Since the W band is targeted, the SIW cut-off frequency of the lowest mode to propagate must be lower than $75GHz$. In [29], it is recommended to use $59GHz$ as the cut-off frequency in order to avoid parasitic effects. With this frequency, it is now possible to compute the a dimension using the following relation [28]:

$$f_{c_{mn}} = \frac{c_{BCB}}{2\pi}\sqrt{(\frac{m\pi}{a})^2 + (\frac{n\pi}{b})^2}$$

where $f_{c_{mn}}$ is the cut-off frequency for a given mn-mode, m and n are the mode indices and c_{BCB} is the speed of light in the medium. By reverting the equation in order to find a and by selecting m and n to propagate the TE_{10} mode in the equation, a is given by:

$$a = \frac{c_{BCB}}{2f_{c_{10}}}$$

Finally, knowing that $c_{BCB} = \frac{3*10^8}{\sqrt{2.5}}$, a is:

$$a = \frac{\frac{3*10^8}{\sqrt{2.5}}}{2 * 59 * 10^9} = 1.608mm$$

A sanity check can be made to be sure no other mode will propagate. The modes to consider are TE_{20} and TE_{01}.
For the TE_{20} mode, the cut-off frequency is given by: $f_{c_{20}} = 2 * f_{c_{10}} = 118GHz$.
For the TE_{01} mode, the cut-off frequency is given by: $f_{c_{01}} = \frac{c_{BCB}}{2b} = \frac{\frac{3*10^8}{\sqrt{2.5}}}{2*16.5*10^{-6}} = 5749.6GHz$.
Both cut-off frequencies are higher than the upper frequency of the W band, so that no spurious modes can propagate.

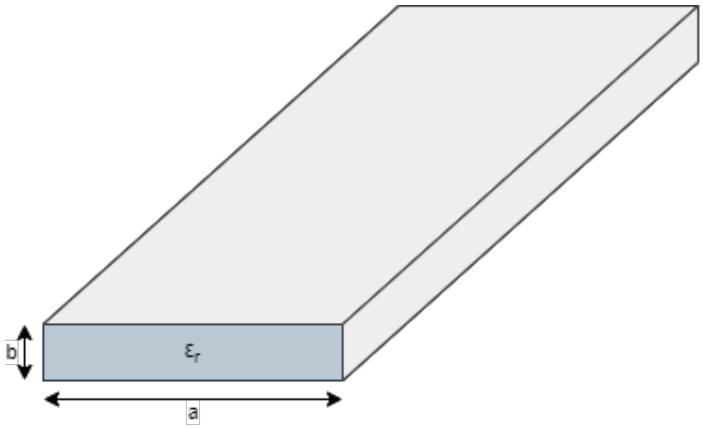

Figure 3.1: Conventional dimensions of a waveguide section. Light grey represents metal and light blue represents dielectric

3.1.3 GCPW design

The other non variable part of the design is the grounded coplanar waveguide. Indeed, the goal is to have a GCPW with an impedance of 50Ω as a reference for the design of the transitions. Again, the parameters that must be determined are those of the section, namely W the width of the center strip, G the width of the space gap between the signal track and the ground track, and W_{wall} the distance from the side wall to the center of the section. The thickness of the GCPW is once again constrained by the substrate choice. It is necessary to differentiate the parameters that determines the impedance of the line from the one that avoids the appearance of parasitic modes. Indeed, the walls positioning does not have much influence on the value of the impedance, they just have to be placed in such a way that they remove parasitic effects.
The different parameters are shown in figure 3.2

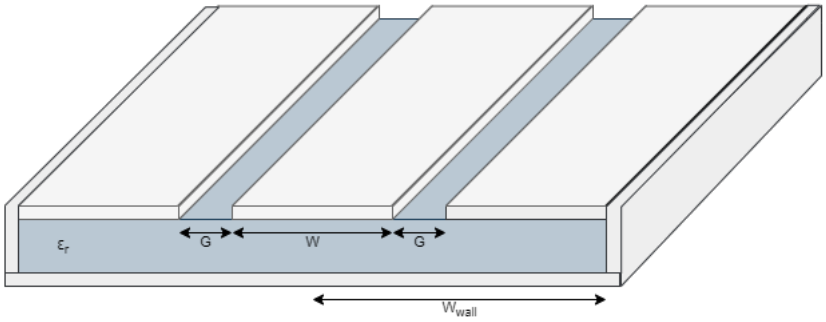

Figure 3.2: Grounded coplanar waveguide with dimensions convention. Light grey represents metal and light blue represents dielectric

Dimensioning

As it was pointed out in section 2.1.4, there is no perfectly-defined theoretical framework for a grounded coplanar waveguide and in any case, a determination using a simulation tool is more simple and accurate.
Nevertheless, one key consideration is worth mentioning before the design by simulation. The impedance of any transmission line is determined by the following relation:

$$Z_c = \sqrt{\frac{L}{C}} \tag{3.1}$$

where Z_c is the characteristic impedance of the line, L is its equivalent inductance and C is its equivalent capacitance.
It can be assumed that the equivalent inductance is linked to the deformation of the field lines while the equivalent capacitance is linked to the distance between metals (the fields are stronger for closer conductors). This means that a smaller substrate increases the capacitance and thus reduces the characteristic impedance of the line. This consideration gives an intuition on how to design the GCPW.
As the grounded coplanar waveguide will be used to measure the device, the constraints associated to the pitch of the probe can be taken as a starting point to determine the parameters. Indeed, the probe has a ground-signal-ground configuration and the center to center distance between two consecutive pins is $100\mu m$. To match the probe requirements, the width of the center strip must be $W = 50\mu m$ and the slot gap must be $G = 55\mu m$. Figure 3.3 represents the constraints due to the pitch of the probe.

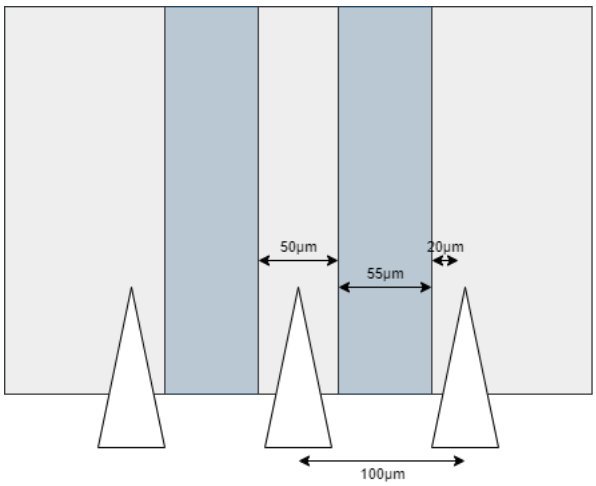

Figure 3.3: Dimension of the GCPW to match requirements of the probe pitch. Light grey represents metal, light blue represents dielectric and white represent the pitch of the probe

Using CST Studio Suite 2021 as simulation tool to design the GCPW, the first try gives an impedance of 39.5Ω. As the value of the impedance is smaller than 50Ω, the center strip width needs to be reduced. After a small iterative process, the dimensions of the grounded coplanar in order to have a 50Ω line without parasitic modes are: $W = 29\mu m$, $G = 65.5\mu m$ and $W_{wall} = 180\mu m$.
Before moving on to the rest of the design, it is important to note that with these dimensions, the grounded coplanar waveguide acts more like a microstrip line. This can be seen on figure 3.4.

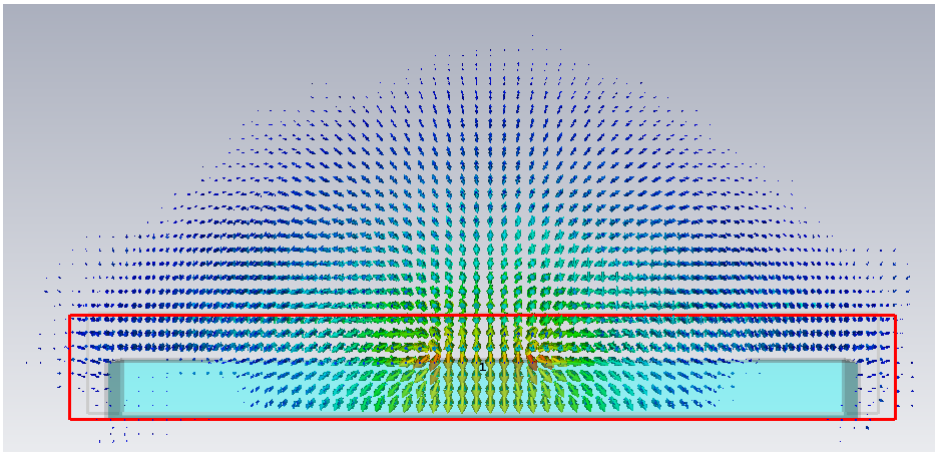

Figure 3.4: Simulated electrical field lines of the designed GCPW in dB scale

3.1.4 CST Studio Suite 2021 as a design tool

The following of the design will be handled with CST Studio Suite 2021. In this context, a quick presentation of the used features is necessary as well as a discussion about the limitations it demonstrates. The focus is made on the features that are related to simulation as they have an influence on the designs.

CST used features for the design of transitions

The first feature of CST that is worth mentioning is the port simulation. The software has multiple way to excite a microwave structure but two are of interest here: the waveguide port and the discrete port. The former is the one that is recommended to use for waveguide and for CPW or GCPW lines. However, according to the line used, the port dimensions have to respect some rules. For a waveguide, it has to correspond to the inner section. For a GCPW, the guidelines are the following: the port begins on the lower ground and has a height equal to the thickness of the substrate added to half the width of the central strip while its width is equal to two or three times the width of the central strip. These guidelines are supposed to ensure a good simulation.
The discrete port on the other hand is mainly used for geometries in which the waveguide port is not usable as the geometry of the structure that will be introduced in chapter 4. To set up a discrete port necessitates to precise a reference impedance and where to put the power precisely. This type of port is therefore a good approximation that sometimes gives better results, but it is possible that more reflection occurs due to lines of different impedance than the port.

The second feature used from CST is the de-embedding or the change of reference plane. Indeed, in the definition of the waveguide port, it is possible to change the reference plane by using the option "distance to reference plane". It then allows to simulate a whole structure but to get the performances of only the part of interest. In the context of this work, this feature is really useful to isolate the scattering parameters of the transition.

The third and last worth mentioning feature is the choice of the solver. CST proposes six different solvers among which two are the main used, namely, the time domain solver and the frequency domain solver. The former is used for time variant problems while the latter is used for problems over a large frequency bandwidth. Moreover, the time domain solver is more accurate for structures that are large compared to the wavelength whereas, on the opposite, the frequency domain solver is more accurate for structures that are small compared to the wavelength. Here, according to the problem, the frequency domain will be used for the design.

Limitations for the design

Even though CST Studio Suite 2021 presents many tools to accurately simulate the designed microwave structures, this software still presents some limitations and two of them are mentioned here.
First, the accuracy of the model is limited by the precision of the solver algorithms. A solution to this problem is to use more frequency simulation points and a smaller meshing but this increases a lot the time duration of a simulation. Therefore, a trade-off must be found between the accuracy of the results and the simulation duration.

The second, and most important limitation of CST is the length before having a stable problem for the GCPW line simulation. Indeed, to have a simulation in which the excitation parameters are correctly set up, the length of the grounded coplanar waveguide has to be very long, about the half of the wavelength. This is a real problem because it distorts the whole simulation. In this context, the change of reference plane that was introduced just above still isolates the transition but the results is dependent on the length of the GCPW line.
In the framework of this work, this problem was observed very late when all the designs were made and the fabrication steps were begun. To honestly represent the work done, the design of the transitions will be described with grounded coplanar waveguide feeders a little over a quarter of the wavelength in length. This will give the key concepts to design the transitions and at the end, transitions with a correct feeding line length will be presented and adapted.

3.2 Design process

The following presents the design process. It is made of successive design tests, trying to improve the performance each time. In the first design trial, key concepts will be identified to make the design and the simulations.

3.2.1 Working principle of the transitions

All the following transitions that will be introduced in the design process try to implement and improve the same working principle.
This principle was introduced in the first chapter and consists in modifying the field profile of the GCPW by means of a transition so that the field lines at the end of the transition correspond to those of the SIW. Moreover, this modification of the fields introduces a transformation of the impedance according to [20]. The following transitions can thus be seen as field and impedance transformers.
These two aspects will then be studied to try to improve the transitions, but as the focus will be on performance indicators, it is important to keep in mind what is happening physically as it will not be repeated when not necessary to make the reading more cumbersome.

3.2.2 Step 1: first design trial

To begin the transition design, a good idea is to start from a transition proposed in the literature. Indeed, instead of reinventing the wheel, the idea is to use a design that offers good results and try to adapt it to the constraints of this work.
The choice is made on the transition from [21]. Among the transitions between a grounded coplanar waveguide and a substrate-integrated waveguide that were studied in chapter 2, this transition offers the best performances over the bandwidth it targets. Moreover, even though the constraints parameters are different, namely, the substrate width and the dielectric, its structure is simple and thus can be manufactured with microfabrication techniques. Therefore, it is a good starting point.
However, it should be mentioned that all transitions, including the chosen one, from a grounded coplanar waveguide to a substrate-integrated waveguide are realized with lines using vias. Nevertheless, as the principle of these transitions is to modify the field profile to make the matching, it should not deteriorate too much the performances of the transitions. As a reminder, the structure of the transition is shown in figure 2.15.

For simplicity, in the following, the continuities of the grounds from the grounded coplanar waveguide in the transition will be named "side grounds" and this transition design will be named "tapered transition with side grounds".

Implementation

Applying the manufacturing process constraints of this work to the chosen design gives the structure of figure 3.5. It is important to note that only the metal and the dielectric are represented and used for the simulation even though they rely on a Silicon layer when it is manufactured. This can be done because the lower ground plane relies on all the Silicon wafer and the structure can hence be considered "isolated".

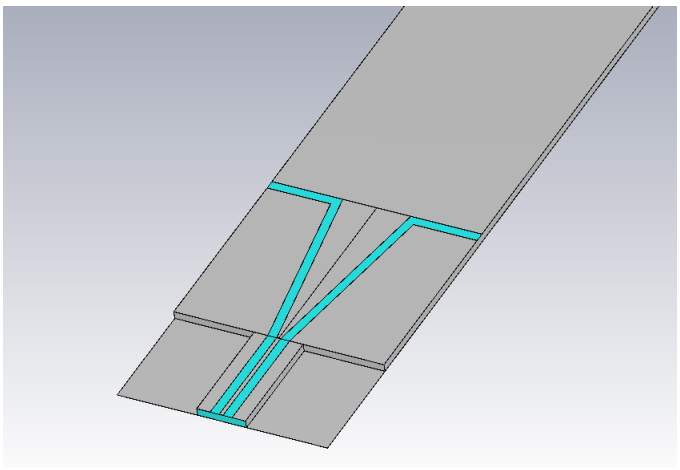

Figure 3.5: Tapered transition with side grounds on BCB substrate-integrated waveguide technology. Grey is metal and blue is the dielectric. The thickness is not to scale.

The study of the literature revealed that for tapered transitions like the one here, the two main parameters to adjust the transition are the taper length and the taper angle.
A schematic top view of the tapered transition with side grounds is shown in figure 3.6. On this schematic, α represents the taper angle and L represents the taper length.

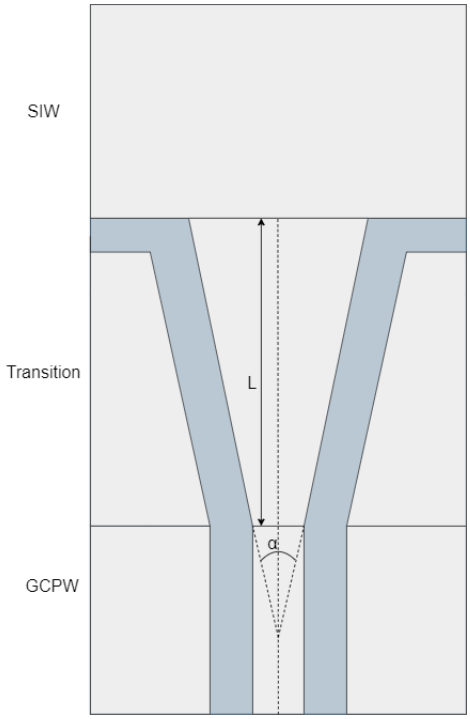

Figure 3.6: Schematic top view of the tapered transition with side grounds indicating the parameters. α is the taper angle and L is the taper length

In a first instance, it can be interesting to use the same parameters as the one from the literature. It thus gives a length $L = \lambda/4$ and an angle $\alpha = 45°$.
The wavelength in the transition can be approximated by an average of two wavelengths, one at the end of the GCPW line and one at the end of the transition. As it has already been mentioned, there is no well-defined theoretical framework for the GCPW in the conditions of

this work. However, it was pointed out in section 3.1.3 that the grounded coplanar waveguide acts more like a microstrip line. An approximation of the effective permittivity can then be brought by equation 2.1.
For the end of the GCPW, this gives:

$$\epsilon_{e_1} = \frac{2.5+1}{2} + \frac{2.5-1}{2}\frac{1}{\sqrt{1+12*16.5/29}} = 2.02$$

It follows that the wavelength at this point is:

$$\lambda_1 = \frac{c/\sqrt{\epsilon_{e_1}}}{f} = 2.283mm$$

where c is the speed of light in the vacuum and f is the central frequency of the band so here, $f = 92.5GHz$ For the second wavelength, as it is supposed that the transition makes a good matching, the wavelength of the waveguide can be considered. According to [29], the wavelength of a waveguide mode for a certain frequency higher than the cut-off frequency of the mode ($f > f_{c_{mn}}$) is given by:

$$\lambda_g = \frac{\lambda_{void}}{\sqrt{1-\frac{f_{c_{mn}}}{f}}}$$

where λ_g is the waveguide wavelength, λ is the wavelength in a medium consisting only of the dielectric ($\lambda = \frac{c}{\sqrt{\epsilon_r}f}$), $f_{c_{mn}}$ is the cut-off frequency of the mode and f is the central frequency of the band ($92.5GHz$). Introducing the respective values in the equation gives:

$$\lambda_2 = \lambda_g = 2.663mm$$

Finally, the approximate wavelength of the transition is:

$$\lambda = \frac{\lambda_1 + \lambda_2}{2} = 2.473mm$$

This value of the wavelength gives the first shot for the transition ($\lambda/4$) and even though this value can be incorrect, it gives an idea to compare with the optimal size of the transition later.

Unfortunately, these parameters do not give the best results. Indeed, the return loss is lower than $10dB$ over the whole W band and even lower than $7dB$ for the first half of the band. On the other hand, the insertion loss is below $2dB$ for most of the band but this is not enough to compensate for the problem of return loss. The return loss and the insertion loss are shown on figure 3.7. To be precise, the scattering parameters are plotted with the reference planes of both excitation ports at the limits of the transition so it is equivalent to a de-embedding to have only the parameters of the transition. The return loss corresponds to the S_{11} parameter with a negative sign and the insertion loss corresponds to the S_{21} parameter with a negative sign.

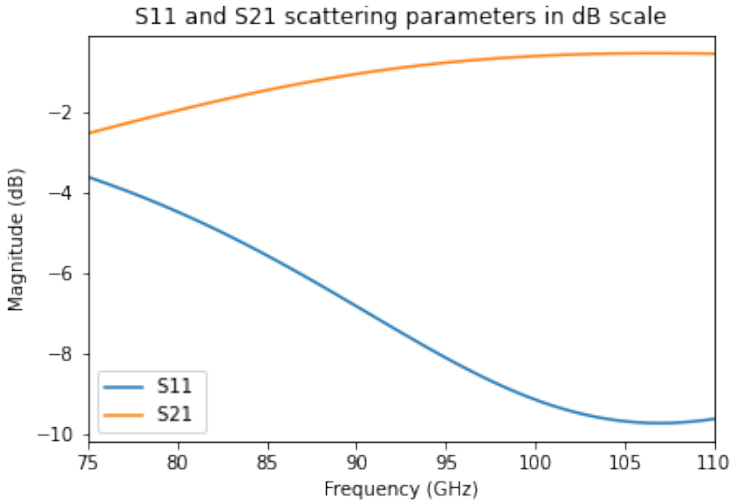

Figure 3.7: De-embedded scattering parameters of the tapered transition with side grounds with a quarter wavelength taper length and $45°$ taper angle

These bad results can be explained by two main factors. First, the design of [21] was developed for a much thicker substrate and for the Ka band. This hence does not correspond to the context of this work. Indeed, with a thicker substrate, the grounded coplanar waveguide really acts like one whereas here, the GCPW line acts more like a microstrip line. Moreover, as it was pointed out earlier, there are errors due to the simulation tool and they play a huge role in the results here. As this second point will be relevant for the entire design process, it will not be recalled hereafter.
Knowing these problems, an iterative process to find the best possible configuration for this transition gives the following parameters and performances: a taper length of $1350\mu m$ and a taper angle of $20°$ for a return loss better than $8dB$ and an insertion loss lower than $0.7dB$. It is worth remembering that these results do not take into account conductor losses.
Figure 3.8 shows the de-embedded scattering parameters of the tapered transition with grounds in two cases: figure3.8a shows the insertion ($-S_{21}$) and return ($-S_{11}$) losses while figure3.8b shows the return and insertions losses for the two configurations considered in this first design step to ease the comparison.
The iterative approach revealed that the match is better when the taper length is increased to just over half the wavelength. It also show that the taper angle must be adapted so that the width of the central strip in the transition covers the most important part of the SIW width. An approximation on this width is that it should be equal to half of the SIW width and it obviously has to be centered.

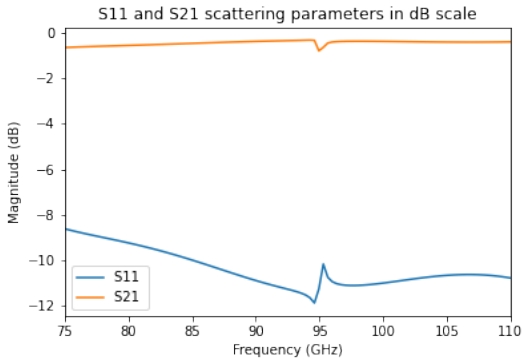

(a) Scattering parameters of the tapered transition with side grounds in its optimal configuration

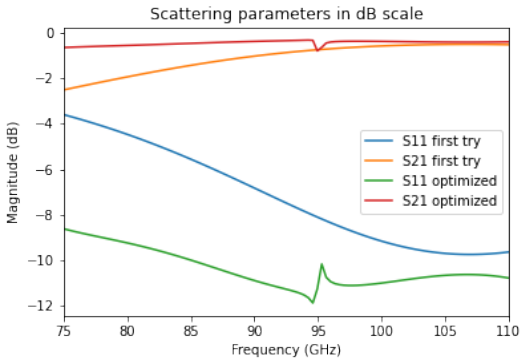

(b) Scattering parameters of the tapered transition with side grounds for the first try and the optimized configurations

Figure 3.8: De-embedded scattering parameters of the tapered transition with grounds. a) with a taper length of $1350\mu m$ and a taper angle of $20°$. b) Scattering parameters of both configuration as a comparison

To remember

This first design attempt allows to identify a number of learnings, of which the following is a list :

1. A tapered design for transitions in W band with a $16.5\mu m$ substrate looks promising. However, a usual approach as the one from [21] does not work because of the GCPW dimensions. Indeed, the microstrip behavior of the grounded coplanar waveguide under the conditions of this work compromises the performance of a GCPW adapted transition design from [21], or at least does not benefit from it.

2. The two main parameters to adapt a classical taper transition are definitely the taper length and the taper angle. The former must be increased to adjust the best matching in the center of the band. The latter must ensure that the width of the end of the transition corresponds to the part of the SIW field profile where the field is maximum (about half the width of the waveguide placed centrally).

3. The variation of the taper length has a bigger impact than the variation of the taper angle.

4. The optimal taper length in the context considered here is slightly higher than half of the wavelength instead of the quarter wavelength expected at first.

3.2.3 Step 2: modifying the taper

Even though the first design does not give good enough results, it allows to understand that the taper can be modified in order to get better results.
It was pointed out that expanding the taper length help to have a better overall matching with a peak around the central frequency. But the key point of this first design attempt is that the side grounds of the structure seem to have no effect, or even degrade the performances of the transition.
To counter this effect, two methods can be studied.

The first way consists in reworking the side grounds to give them a shape similar to what is done in [2] or [19] and the second is to simply remove them.
Both ideas will be tried to find out which one provides the best results

Modified side grounds

To modify the structure, the side grounds are extended until the SIW and they are parameterized to be able to change their angle. Moreover, the sidewalls are also modified to they are diagonal in shape going from the end of the GCPW to the start of the SIW sections. This structure is in fact shaped so it resembles some that can be found in the literature as in [2] and [19]. It is shown on figure 3.9.

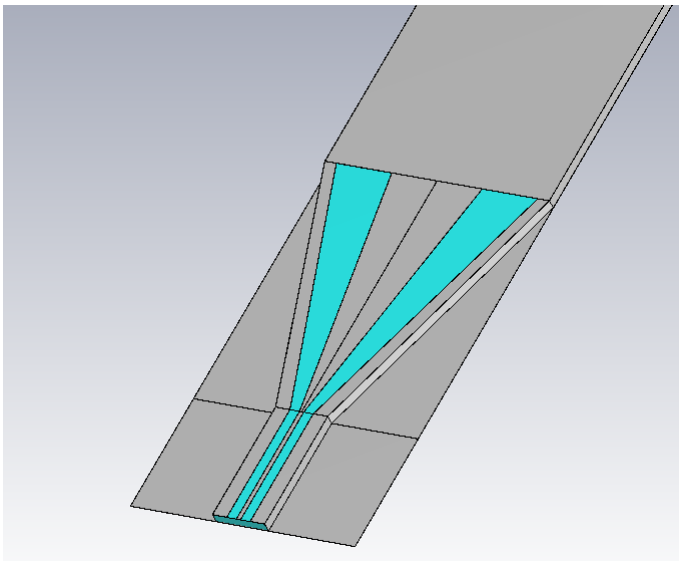

Figure 3.9: Tapered transition with modified side grounds on BCB substrate-integrated waveguide technology. Grey is metal and blue is the dielectric. The thickness is not to scale.

This transition design adds an extra variable which is the tapering angle of the side grounds. It is named β. Figure 3.10 shows a schematic top view of the new transition with the different parameters including β.

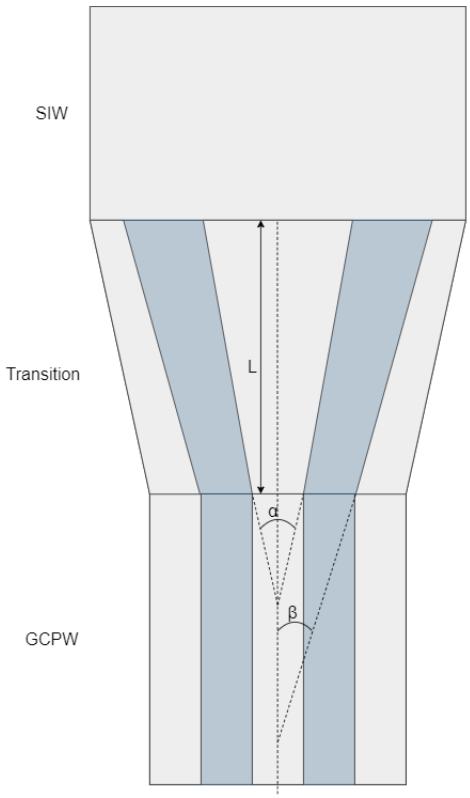

Figure 3.10: Schematic top view of the tapered transition with modified side grounds indicating the parameters. α is the taper angle, L is the taper length and β is the side grounds taper angle

It is now necessary to determine the impact of the β parameter on the performance.
The previously found optimal parameters could be used for the central taper as a starting point. However, it turns out they are not optimal here. The same iterative process as the one in the first design step is thus made to find the new optimal configuration keeping a constant side grounds tapering angle β. The process is not detailed but it shows that the best parameters for the central taper are a taper length $L = 1500\mu m$ and a taper angle $\alpha = 20°$. The length is this time a little longer than the half wavelength.
With these parameters fixed, it is now possible to perform simulations with a variable side grounds taper angle β. Graphs presenting the results are shown in figure 3.11. Figure 3.11a shows the return loss ($-S_{11}$) and figure 3.11b shows the insertion loss.

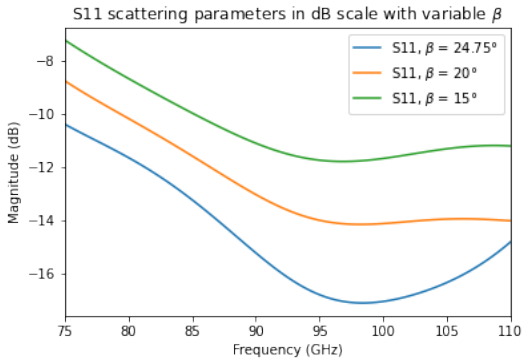

(a) S_{11}

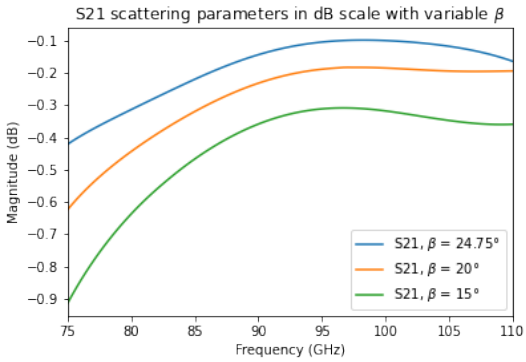

(b) S_{21}

Figure 3.11: De-embedded scattering parameters of the tapered transition with modified side grounds. Sweep on the β angle

The simulations show that the best configuration is the one where the grounds are the least significant, that is, when the tapering angle of the side grounds is maximal. Indeed, the structure with $L = 1500\mu m$, $\alpha = 20°$ and $\beta = 24.75$ shows return loss better than $10dB$ and insertion loss lower than $0.4dB$ on almost the entire W band
This result reinforces the intuition that a transition without the side grounds could really be the best one.

Removed side grounds

Removing the side grounds in the transition means that it is now closer to a microstrip to substrate-integrated waveguide transition than a transition from a GCPW to a SIW. The structure is shown in figure 3.12.
It is worth mentioning that this structure does not introduce any new parameter.

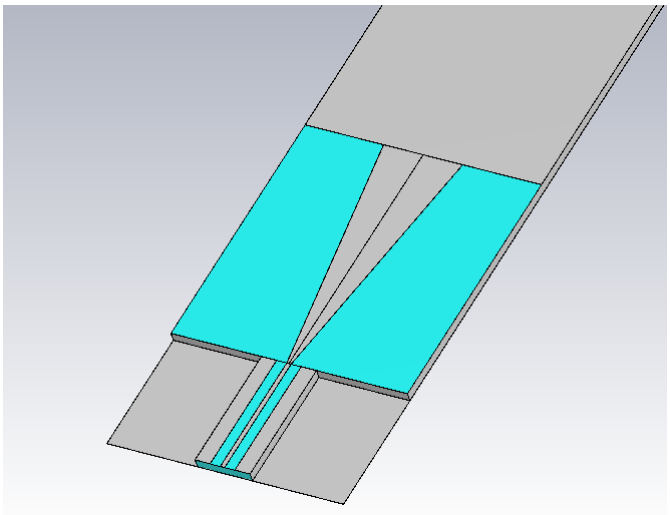

Figure 3.12: Tapered transition without side grounds on BCB substrate-integrated waveguide technology. Grey is metal and blue is the dielectric. The thickness is not to scale.

To ensure that this structure modification improves performance, a simulation with the same taper length and angle as the first test is performed. This simulation presents small improve-

ments compared with the optimal results of the first design step, especially at high frequencies showing the uselessness of the side grounds. A comparison graph of the optimal results from the first design step and the simulated results with the same parameters without the side grounds is shown in figure 3.13.

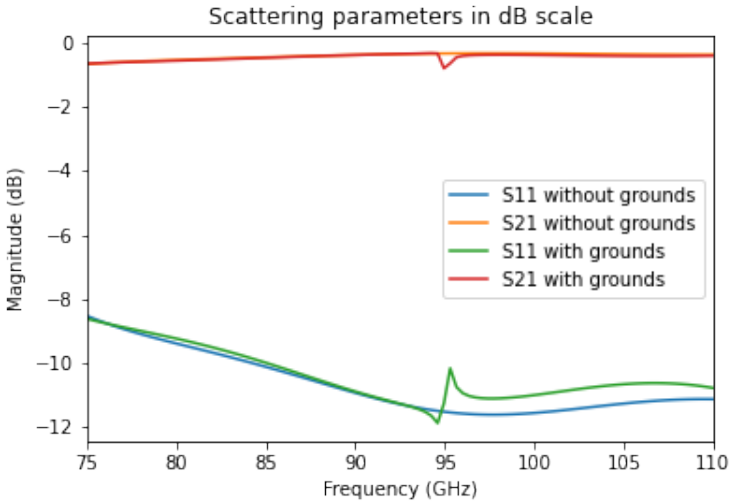

Figure 3.13: Comparison of the de-embedded scattering parameters of the tapered transition with and without side grounds.

Furthermore, since the idea is to design the best possible transition for the entire W band on the BCB substrate-integrated waveguide technology, an optimization of this transition is done. It is again performed by an iterative method that consists of simulating different sets of parameters to determine trends, and then, following these trends to find the best possible configuration.
Surprisingly, the emerging trend is that the taper length needs to be increased to have a better matching on the entire band. However, this also moves the peak of performance to higher frequencies.
The optimal parameters for this transition are: $L = 1600$ and $\alpha = 17.5°$. These parameters result of the trend identified above for the taper length and from the fact that the taper angle needs to be reduced to keep the same width at the end of the transition when the length increases.
This configuration gives return loss better than $10dB$ on the whole band and even better than $15dB$ after $87.5GHz$ while insertion loss is lower than $0.4dB$ over the entire band. Figure 3.14 shows the results for this optimal configuration as well as the ones with the previous optimal configuration.

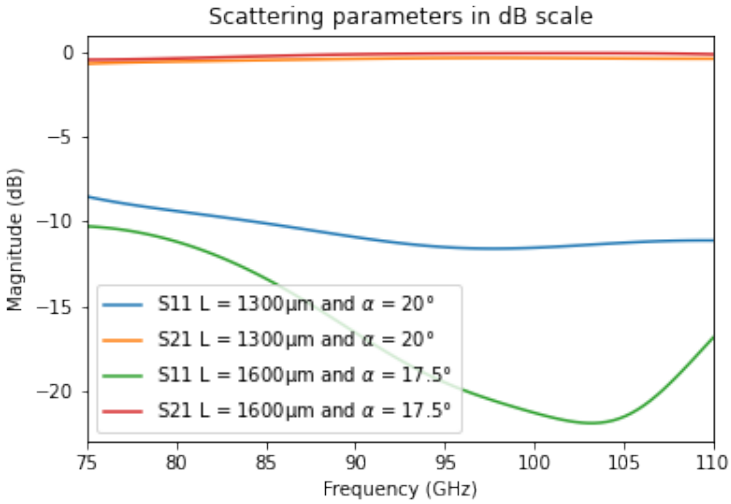

Figure 3.14: De-embedded scattering parameters of the tapered transition without side grounds: comparison between the previous and the new optimal parameters

To initiate the next step of the design process, the scattering parameters of the transition can also be shown in the Smith chart. This is done for the optimal transition of this step and it gives the curve of figure 3.15.

A quick review of the Smith chart is in order. When the S_{11} parameter is in the upper half of the Smith chart, the studied device presents an inductive behaviour. On the opposite, When the S_{11} parameter is in the lower half of the Smith chart, the studied device presents a capacitive behaviour. For the device to be match, the S_{11} needs to be at the center.

Given the curve from figure 3.15, the transition presents an inductive behaviour.

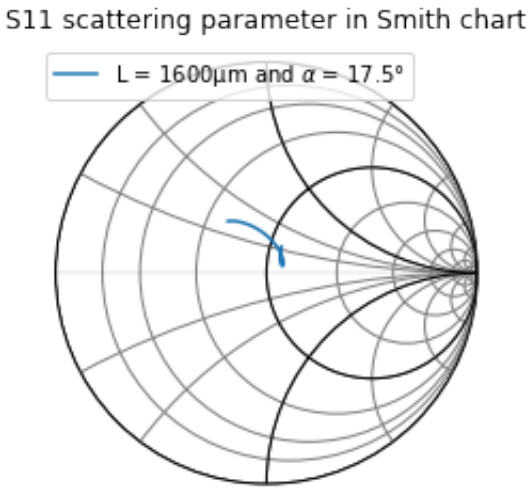

Figure 3.15: De-embedded scattering parameters of the tapered transition without side grounds in the Smith chart

To remember

The second step of the process design reveals the following key elements:

1. The side grounds prove to be annoying within the framework of this paper.
2. The transition without side grounds is even better than the transition with modified ground (higher overall return loss).
3. The transition without side grounds has an inductive behaviour.

3.2.4 Step 3: shape redrawing

The study of the transition without side grounds proves to be promising. However, its inductive nature was pointed out at the end of the previous design step.
One way to counter this is to reshape the transition to have an elliptical shape. This shape ensures that the impedance change is not too abrupt. This also softens the curvature of the field lines which reduces the inductive character.
To form this new transition shape, an ellipse is removed from the initial taper. Thus, the parameters of the transition do not change fundamentally and can be optimized in the same way as in the previous steps. This manipulation and the parameters of the transition are shown in figure 3.16 and the structure of the new transition, named "elliptic transition", is shown on figure 3.17 in three dimensions.

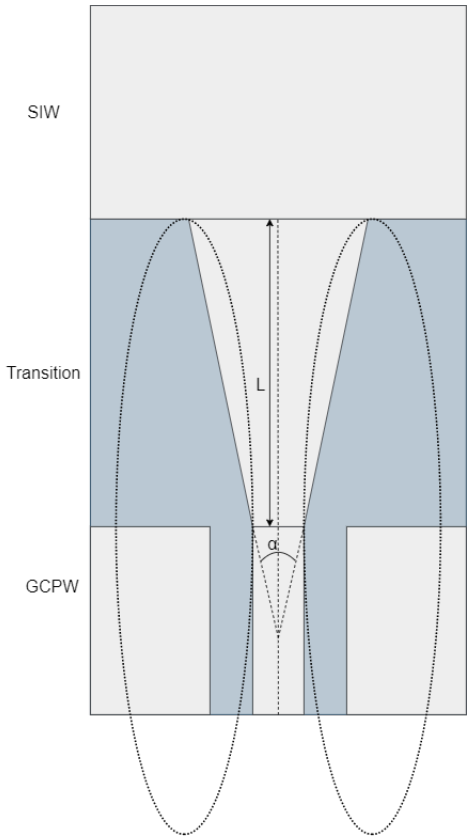

Figure 3.16: Schematic top view of the elliptical shaped transition indicating the parameters. α is the taper angle and L is the taper length.

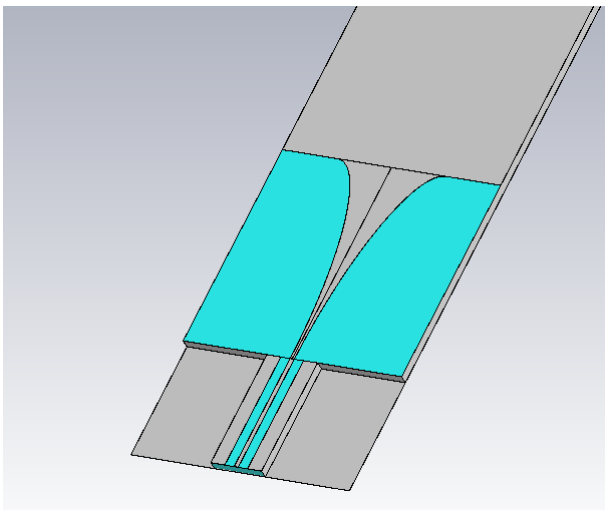

Figure 3.17: Elliptic transition on BCB substrate-integrated waveguide technology. Grey is metal and blue is the dielectric. The thickness is not to scale.

Using the same length as for the last transition and optimizing the angle to get a good match, the results in figure 3.18 are obtained: return loss better than $10dB$ over the entire band with a $23dB$ peak at $86GHz$ and insertion loss lower than $0.5dB$ over the entire band with a $0.5dB$ peak at $86GHz$.
These results show that the shape change has removed the inductive character of the transition.

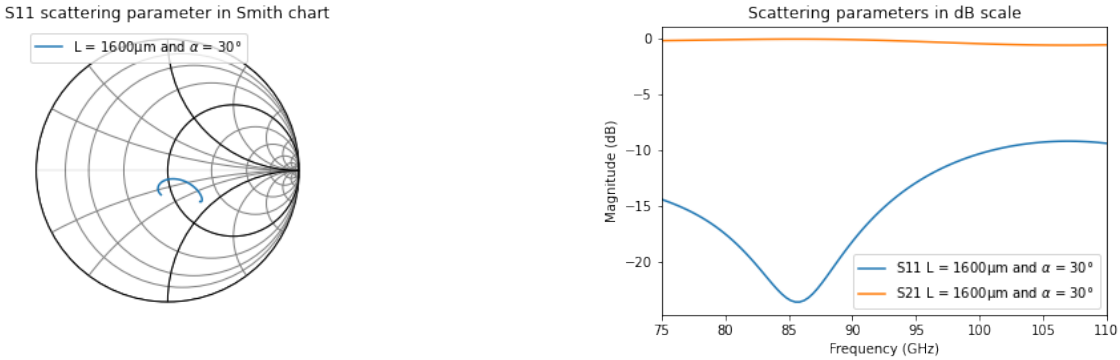

(a) S_{11} in Smith chart

(b) S_{11} and S_{21} in dB scale

Figure 3.18: De-embedded scattering parameters of the elliptic transition

To remember

The key point observed here is that the new elliptic shape improves the matching by removing the inductive character of the transition. However, the matching is still not perfect because the S_{11} parameter is now in the lower half of the Smith chart (inductive part).

3.2.5 Step 4: adding a discontinuous element and revising the ellipse

Up to this point, two transition designs show good enough results. The tapered transition without side grounds and the elliptic transition.
To further improve the performance of both transitions, last modifications are made.

For the tapered transition without side grounds only a discontinuous element is added to the transition.
For the elliptical transition, a discontinuous element is added to the transition and the way the elliptical shape is modeled is changed.

Tapered transition with discontinuous element and without side grounds

The new transition shape is shown in figure 3.19 and a top view with the new design variables associated to the discontinuity is shown in figure 3.20. L_c, W_c and ΔL are respectively the length, the width and the relative position with respect to the GCPW of the discontinuous element.
The idea behind adding this discontinuous element to this transition is to add a capacitive element. It is the principle used in stepped-impedance filters. Indeed, it can be shown that a rectangular discontinuity as the one here acts as a capacitive element as long as its length is much smaller than a quarter wavelength ($L_c << \lambda/4$)) [30].
This trick is another way to counteract the inductive effect highlighted in step 2. However, it should be mentioned that it is relatively narrowband. Therefore, another iterative process to determine the best possible set of the discontinuity and the taper parameters is made.

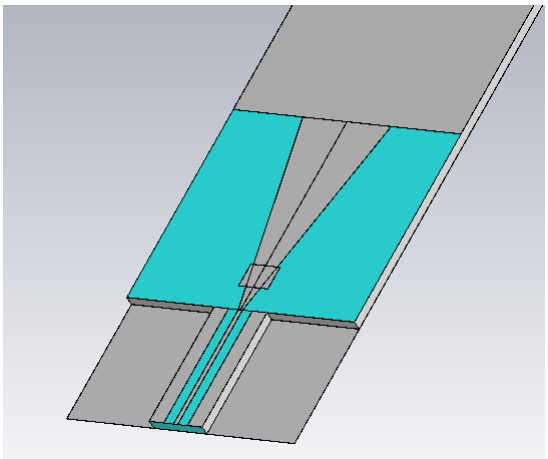

Figure 3.19: Tapered transition without side grounds with capacitive element on BCB substrate-integrated waveguide technology. Grey is metal and blue is the dielectric. The thickness is not to scale.

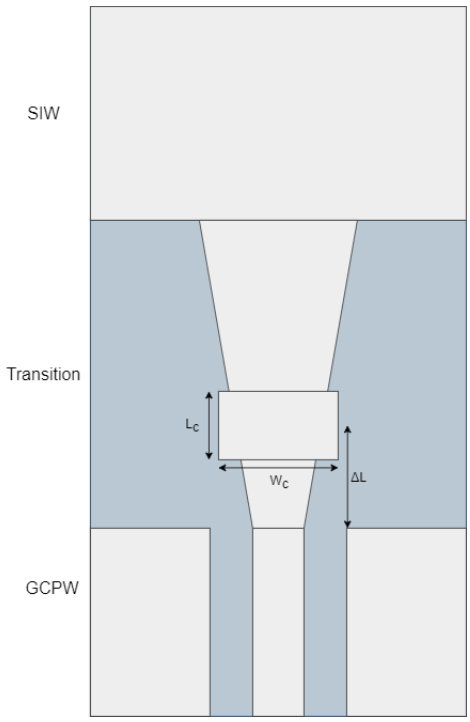

Figure 3.20: Schematic top view of the tapered transition with discontinuous element and without side grounds indicating the new design parameters

After some iterations, the best set of parameters for the tapered transition with discontinuous element and without side grounds is the following: $L = 1700\mu m$, $\alpha = 15°$, $L_c = 60\mu m$, $W_c = 70\mu m$ and $\Delta L = 35\mu m$. It is worth noting that the discontinuity proves to be better when positioned near the GCPW in the case of the tapered transition.
This set produces the following results: return loss better than $12dB$ over the entire band with even $15dB$ from 81 to $110GHz$ and insertion loss lower than $0.3dB$ over the entire band with even $0.15dB$ from 81 to $110GHz$.

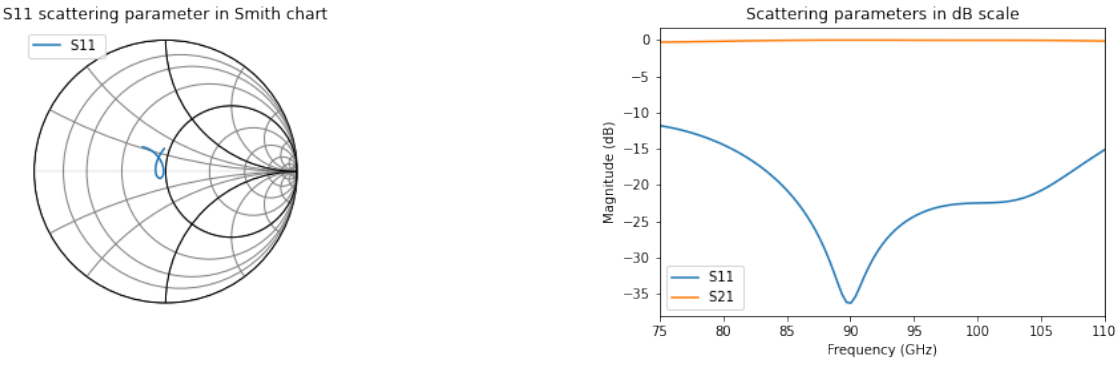

(a) S_{11} in Smith chart

(b) S_{11} and S_{21} in dB scale

Figure 3.21: De-embedded scattering parameters of the tapered transition with discontinuous element and without side grounds. $L = 1700\mu m$, $\alpha = 15°$, $L_c = 60\mu m$, $W_c = 70\mu m$ and $\Delta L = 35\mu m$

Elliptic transition with discontinuous element and modified elliptic modeling

The first change for the elliptic transition is the way the ellipse modeling is done. In order to smooth the end of the transition, the ellipse can be drawn as shown on the schematic top view from figure 3.22. This adds a new variable named $\Delta L_{ellipse}$ and allows to reduce the capacitive aspect introduced in the previous design step.
The other change is the same than for the tapered transition, that is, adding a discontinuous element to the transition. However, here, it is more a way to have an adjustable reactive element than a pure capacitive element as it was the case for the tapered transition. This change is shown in figure 3.23. The parameters for this discontinuity are the same than in 3.20.

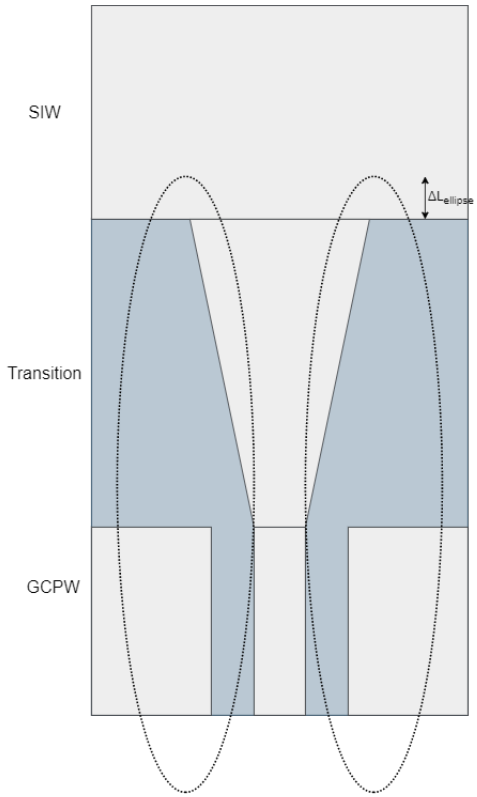

Figure 3.22: Schematic top view of the elliptical shaped transition indicating the new design variable $\Delta L_{ellipse}$

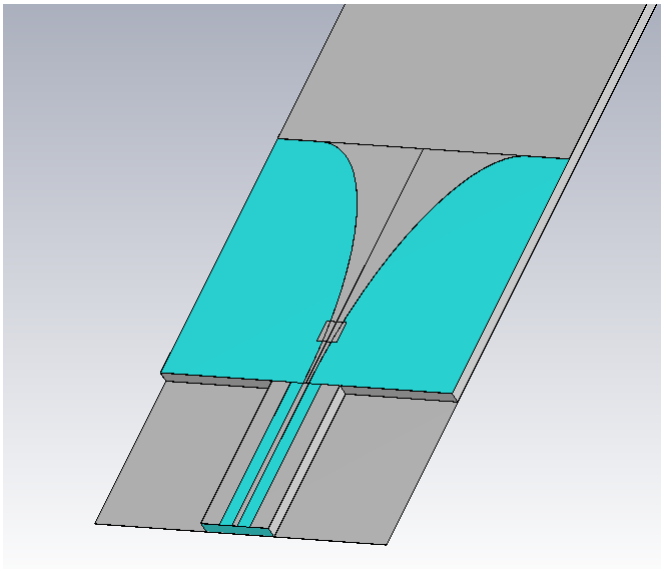

Figure 3.23: Elliptic transition with discontinuous element on BCB substrate-integrated waveguide technology. Grey is metal and blue is the dielectric. The thickness is not to scale.

As for all the other steps, it is now necessary to optimize the performance according to the design parameters.
After observing the effects of the parameters on the performance and many iterations, the set of parameters that optimizes the transition are the following: $L = 1500\mu m$, $\alpha = 38°$, $L_c = 120\mu m$, $W_c = 80\mu m$, $\Delta L = 285\mu m$ and $\Delta L_{ellipse} = 75\mu m$. This configuration leads to the following performances: return loss better than $12dB$ and insertion loss lower than $0.24dB$ over the entire W band. The performance is even better on the frequency range from 75 to $103GHz$ where return loss is above $15dB$ and insertion loss is below $0.15dB$.
To ease the reading, only the results for the best set of parameters of both changes are presented in figure 3.24.

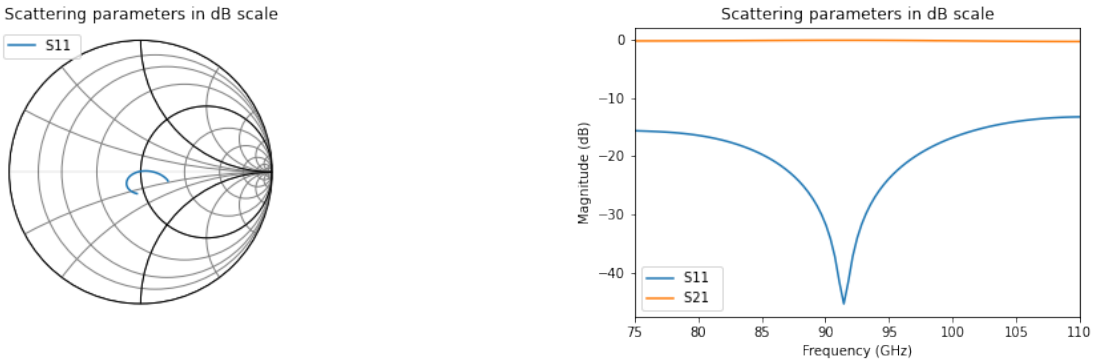

(a) S_{11} in Smith chart

(b) S_{11} and S_{21} in dB scale

Figure 3.24: De-embedded scattering parameters of the reshaped elliptic transition with discontinuous element. $L = 1500\mu m$, $\alpha = 38°$, $L_c = 120\mu m$, $W_c = 80\mu m$, $\Delta L = 285\mu m$ and $\Delta L_{ellipse} = 75\mu m$

3.2.6 Step 5: simulating conductor losses

The last step to finish the design process is to simulate the two optimal transitions from the previous step including conductor losses.
To do this, the metal used for the simulations, which is a perfect conductor, is replaced by aluminum.
In theory, this should have a positive impact on return losses since they will be increased and a negative impact on the insertion loss since, once again, it will be increased.
Figure 3.25 shows that this is true for the tapered transition with discontinuous element and without side grounds.
Figure 3.26 shows that this is also true for the elliptic transition with discontinuous element and modified elliptical shape even though it is not clear for the S_{11} parameter because of the approximations of the simulations.

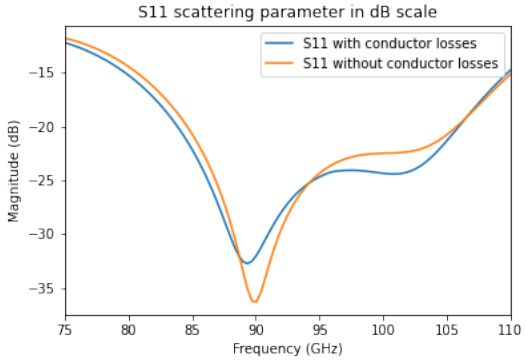

(a) S_{11} in dB scale

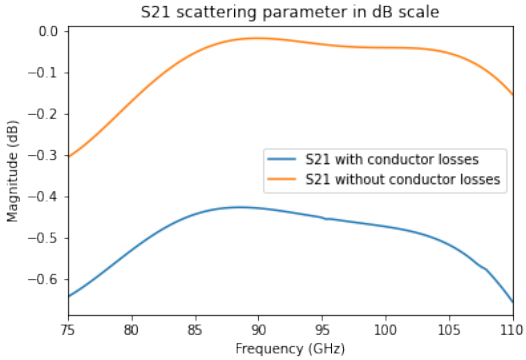

(b) S_{21} in dB scale

Figure 3.25: De-embedded scattering parameters of the tapered transition with discontinuous element and without side grounds: comparison with and without conductor losses

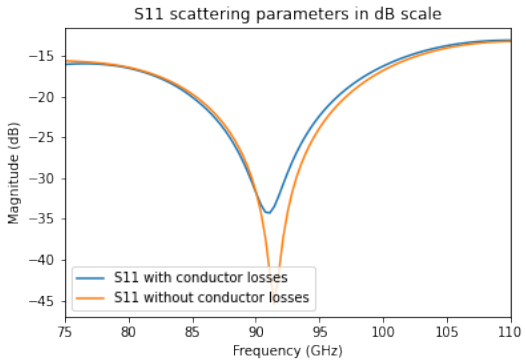

(a) S_{11} in dB scale

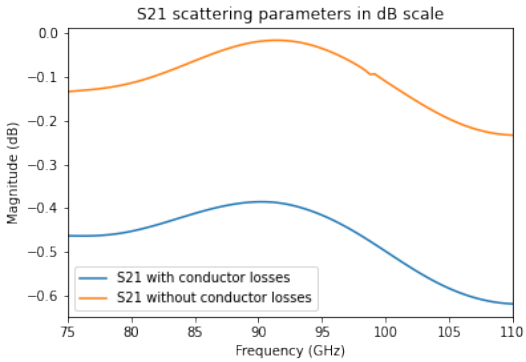

(b) S_{21} in dB scale

Figure 3.26: De-embedded scattering parameters of the elliptic transition with discontinuous element and modified elliptical shape: comparison with and without conductor losses

3.3 Corrected simulations

In the section 3.1.4, it was mentioned that a bug in simulations was detected late in the progress of this work. Indeed, the results presented throughout this chapter proved to be variable as a function of the length of the GCPW line as long as the line was not long enough even though de-embedding was done.
The purpose of this section is to show what the the previously designed transitions look like with a sufficiently long GCPW line length (greater than half the wavelength).
In addition, the design of the tapered transition is re-adapted in order to be able to make two types of transitions and to cover one case without considering the bug and one with.

3.3.1 Simulations with GCPW length equal to the wavelength

Figures 3.27 and 3.28 show the scattering parameters simulated with length of the GCPW equal to the wavelength for, respectively, the final elliptic and tapered transitions.
Unfortunately, the results are not as good as before.
The elliptic transition still manages to have return loss higher than $9dB$ over the entire band and even higher than $10dB$ on most of the band. It also has insertion loss lower than $0.9dB$ over the entire band.
The tapered transition, on the other hand, shows worse results. It only has return loss higher than $8dB$ for the entire band even though it has a peak to $30dB$ for $101GHz$. The return loss is barely below $1.1dB$.

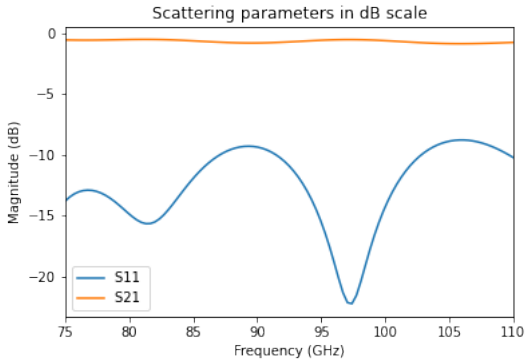

Figure 3.27: De-embedded scattering parameters of the elliptic transition with discontinuous element and modified elliptical shape: consideration of the bug

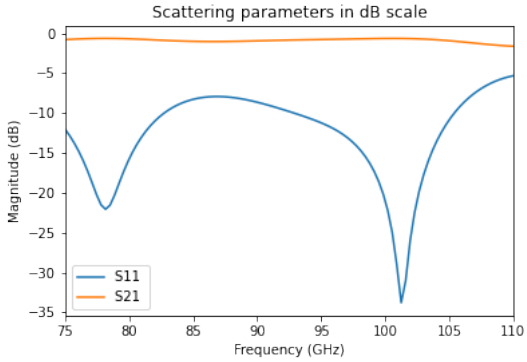

Figure 3.28: De-embedded scattering parameters of the tapered transition with discontinuous element and without side grounds: consideration of the bug

3.3.2 Re-adapted tapered transition

Considering a length for the GCPW that provides results without bugs, the final tapered transition design is re-adapted. This is done by performing a final iterative simulation process to find the optimal set of parameters in this case. This results in the following set of parameters: $L = 675\mu m$, $\alpha = 20°$, $L_c = 70\mu m$, $W_c = 120\mu m$ and $\Delta L = 50\mu m$. These allow to obtain the following performances: return loss better than $10dB$ on the quasi-totality of the band and insertion loss lower than $0,8dB$ except for the frequencies higher than $106GHz$. These results are shown in figure 3.29.

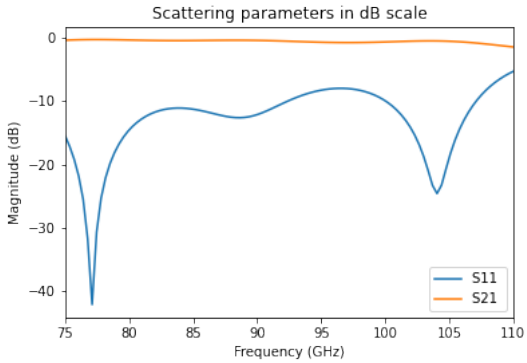

Figure 3.29: De-embedded scattering parameters of the tapered transition with discontinuous element and without side grounds: optimization with a wavelength GCPW length

Chapter 4

Fabrication

The purpose of this chapter is to discuss and prepare the fabrication of the transitions designed in the previous chapter. This will be done using a BCB substrate-integrated waveguide process of fabrication developed by Nicolas Vanpée in his own master's thesis.
This chapter begins with a brief description of the manufacturing process. Then, it will discuss the design of the structures needed to do a TRL (thru-reflect-line) calibration that will allow de-embedding on the measurements. It will also explain the modification that must be made to the GCPW line in order to perform the measurements. Finally, it will present the mask that will be used in the fabrication. It is also important to note that the fabrication will only cover the last two transitions discussed, namely the final elliptical transition and the final tapered transition.

4.1 Brief introduction to the manufacturing process

The manufacturing process developed by Nicolas Vanpée in the context of his master's thesis was created around the use of a BCB substrate. To be precise, it uses a non-photosensitive benzocyclobutene (BCB). This one is deposited on a layer of aluminum, which is used as ground plane, itself deposited on a layer of Silicon.
The following list presents the different steps of the manufacturing process without going into detail:

1. Aluminum deposition
2. Benzocyclobutene deposition
3. Aluminum deposition: aluminum layer used as an hard mask for the etching of the BCB
4. Lithography (negative)
5. Aluminum etching: wafer is immersed in acid to dissolve the aluminum which is not protected by the resin
6. BCB etching: BCB is etched thanks to a plasma of 2 gas (O2 and SF6)
7. Aluminum deposition
8. Lithography (positive)

9. Aluminum etching

10. Removing of the photo resin

In this list, three steps are important to note.
Steps 3 and 7 because they justify the design of a mask. Indeed, the manufacturing of the transition is done using a mask that allows to give the desired shape to the BCB and to the aluminum.
Step 9 because it can be problematic and therefore requires special attention. In this step, the aluminum is etched but this manipulation is difficult to achieve in practice and there is a great risk of over etching the aluminum. This over etching is normally estimated to $0.5\mu m$.

4.2 Modification of the GCPW line

In order to measure the structure, the access is made via the GCPW line. However, as mentioned in section 3.1.3, the dimensions of the line had to be modified to reach an impedance of 50Ω. This implies that they are no longer adapted for placing probes on the line.
Figure 4.1 from section 3.1.3 is shown once again here to recall the required dimensions needed perform the measurements.

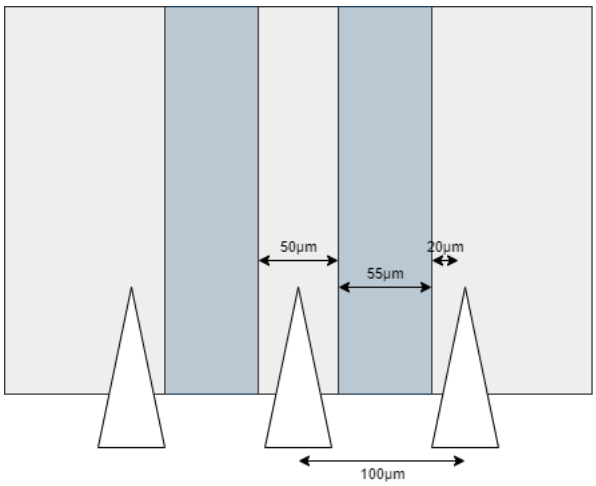

Figure 4.1: Dimension of the GCPW to match requirements of the probe pitch. Light grey represents metal, light blue represents dielectric and white represent the pitch of the probe

To meet these requirements, an additional section named pad is added to the central strip of GCPW line. This pad has the right dimensions to be able to perform the measurements.
This addition implies the appearance of a transition section of $10\mu m$. However, since its size is very small compared to the wavelength, it can be ignored.

Due to the manufacturing process, the edge of the line also needs to be changed. Indeed, to avoid having a metalization on the beginning of the GCPW line, it is necessary to manually add metal further.

The two changes are shown from a top view in figure 4.2

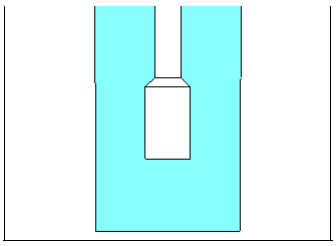

Figure 4.2: Modified beginning of the GCPW line

4.3 Design of the structures for a TRL calibration

In order to have a greater precision during the measurements by removing the parasitic effects of the accesses and in order to be able to make de-embedding to extract the measured performances from the transitions, it is necessary to use a TRL type calibration.
To be precise, here, an mTRL (Multiline TRL) calibration is used. A complete study of the operating principles of TRL and mTRL calibrations is beyond the scope of this work and more information can be found in [31–34].
Instead, the essential points for using the mTRL calibration are explained here. They are then applied to the context of this work

4.3.1 Quick introduction to mTRL calibration

The mTRL calibration, for "Multiline Thru-Reflect-Line calibration", is, as its name indicates, a calibration technique to remove the undesirable effects of probes appearing during the measurements and also to perform de-embedding on the measurements.
For this second point, the mTRL allows in fact to determine the propagation constant and thus to shift the reference plane of the scattering parameters to the desired location.
Indeed, when the scattering matrix $\mathbf{S_1}$ (the matrix of the scattering parameters) is determined at some place, it is possible to know it $\mathbf{S_2}$ at distance l assuming a deduced propagation constant γ by using the following relation:

$$\mathbf{S_2} = \mathbf{S_1} \times e^{\gamma l}$$

The TRL calibration also determines the characteristic impedance.
In reality, the mTRL algorithm is more complete and complicated but it gives an idea of how to do de-embedding with this calibration.

Finally, to use the mTRL calibration, different lines are needed, namely, a Thru which is the reference line, a Reflect which can be a line ending in short circuit or open circuit, and Lines (at least two) of different lengths than the Thru.
The choice of short circuit or open circuit is made according to the ease of implementation.
For the length of the Lines, the goal is to determine lengths that maximize the phase delay between the Lines and the Thru over the desired bandwidth. The rule of thumb, is to have a phase-delay higher than $30°$ over the entire targeted frequency band.

4.3.2 Application of the mTRL design

In the context of this work, the mTRL is used to make a de-embedding on the measurement to extract the scattering parameters of the transition.

This requires to apply the mTRL to the GCPW access lines and to the entire back-to-back structure.

mTRL for the GCPW access lines

First, it is necessary to choose a Thru length. This length is the double of the GCPW access length, so it is $400\mu m$ long.
Then, since the access line is a grounded coplanar waveguide, it is easier to implement an open circuit as the Reflect.
Finally, using a script implementing the mTRL algorithm, the two lengths of the Lines are determined so they maximize the phase delay with respect to the Thru over the W-band. These lengths are $900\mu m$ and $1000\mu m$.

To illustrate one element of the mTRL, the Thru is shown in figure 4.3.

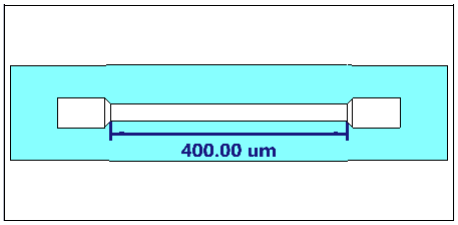

Figure 4.3: GCPW Thru

mTRL for the whole back-to-back structure

The different elements of the mTRL are determined with exactly the same procedure for the whole back-to-back structure.
This gives a Thru of $5000\mu m$ and Lines of $5500\mu m$ and $5600\mu m$ long.
However, since the main line here is a substrate-integrated waveguide, the Reflect chosen is a short circuit to simplify the fabrication. Once again, the Thru line is shown to illustrate in figure 4.4.

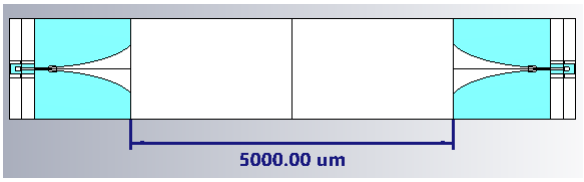

Figure 4.4: Back-to-back Thru structure

4.4 Presentation of the mask

Now that all the changes have been made and that a line selection has been made to perform an mTRL calibration, a mask can be designed.
This mask is co-designed with Nicolas Vanpée and that is why some of the structures that are present are not used in this work.

The complete mask is presented in figure 4.5.
As this figure suggests, the mask consists of repeating subparts called dies. A die contains the structures that are to be studied. The usefulness of repeating the same pattern in several places of the mask is to be able to take advantage of several measurements of the same structure in case there should be an etching problem at a specific place during the manufacturing process.

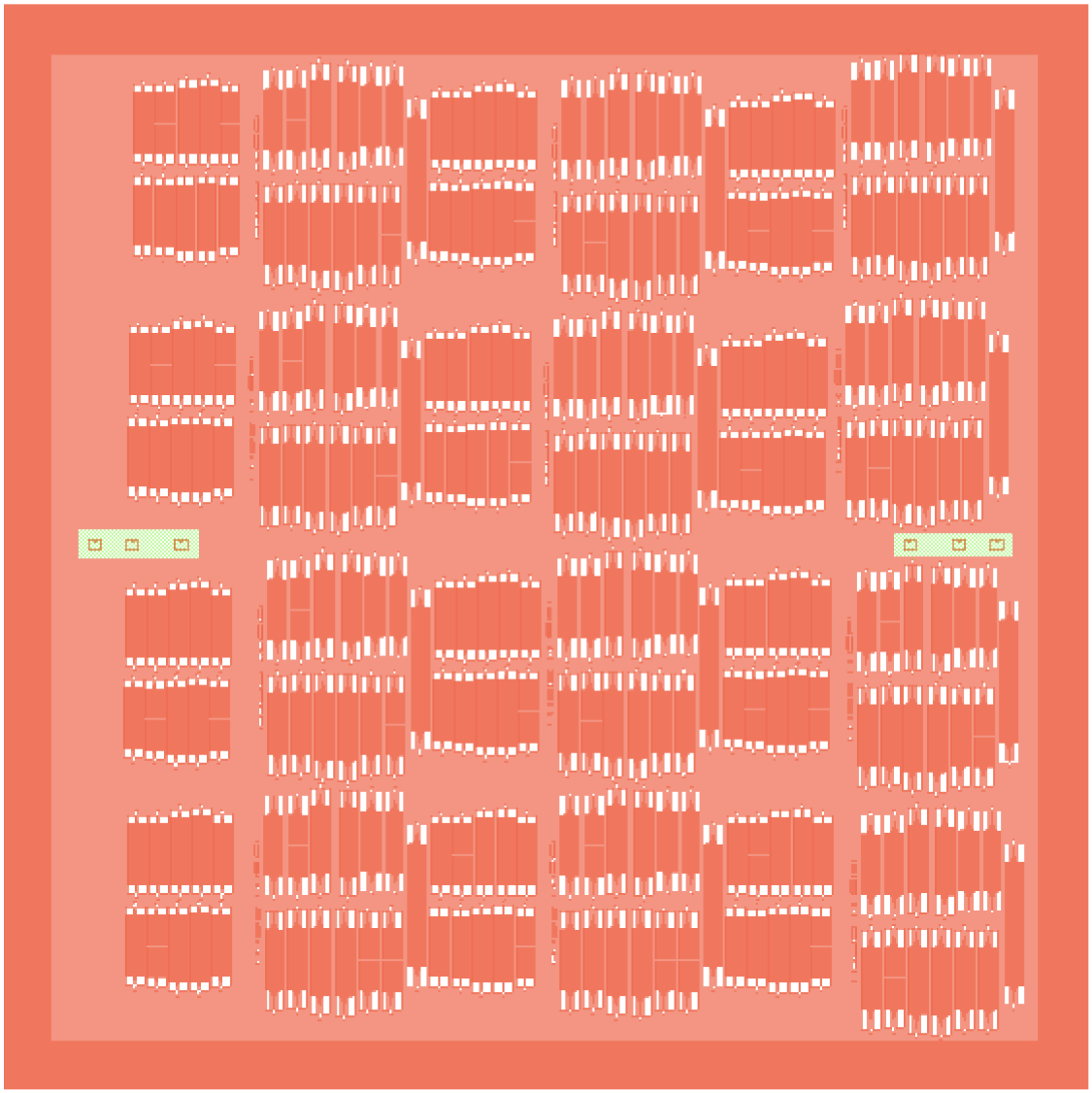

Figure 4.5: Complete mask used for manufacturing

The content of a die is shown in figure 4.6.
Once again, a pattern seems to be repeated. Indeed, except for the long back-to-back transition, the upper half and the lower half of the die are similar. However, the upper half contains the designed structures and the lower half contains these structures but their metalized parts are wider by $1.5\mu m$. This is an anticipation of the over-etching that was mentioned in the description of the manufacturing process by taking even a margin of $1\mu m$.

Nevertheless, each of these two halves are made up of the same kind of structures.
From left to right, there are:

- the different GCPW structures for the mTRL calibration (a clock-wised rotated zoom is

shown in figure 4.7);

- the Thru, the Reflect (short circuit), the Line 1 and the Line 2 of the final elliptic transition in a back-to-back configuration;
- two structures that are for the Master's thesis of Nicolas Vanpée
- a final elliptic transition in a back-to-back configuration with a longer SIW section (common to the two halves of the die);
- the Thru, the Reflect (short circuit), the Line 1 and the Line 2 of the final tapered transition in a back-to-back configuration;

Finally, green rectangles can be seen in figure 4.5. These are alignment markers that are used to ease the measurements.

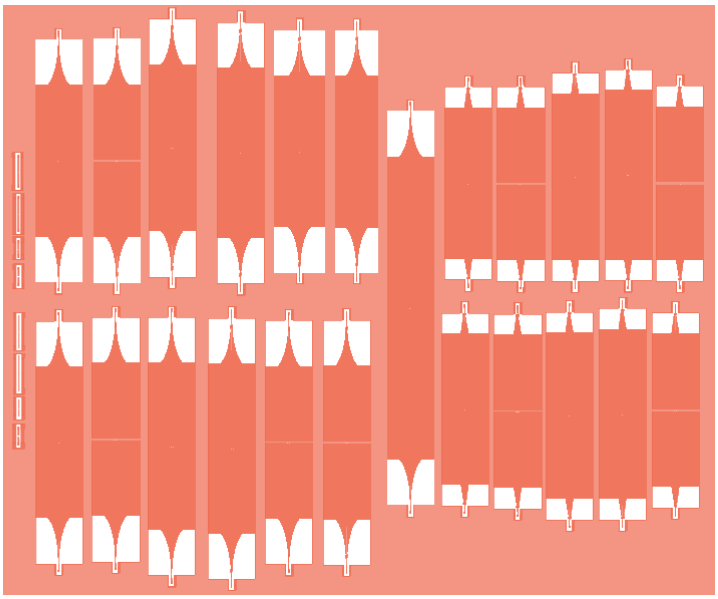

Figure 4.6: Content of a die

Figure 4.7: Zoom on clock-wised rotated Back-to-back GCPW structures for the mTRL calibration from the mask. From left to right: Reflect (open circuit), Thru, Line 1 and Line 2

Chapter 5

Testing

The purpose of this chapter is to present the results of the fabrication of the transitions and their performance.
To do so, the fabricated structures will first be shown and a problem related to the fabrication degrading the performance measurement will be identified.
Then, the de-embedded results of the measurements will be presented as well as how they have been obtained. Finally, a small discussion of these results will be made.

5.1 Fabricated structures and problems for the measurements

The fabricated transitions are shown in figure 5.1 where the images have been enlarged to allow the microscopic structures to be seen.
These images show that the shape of the transitions was well designed during the manufacturing process.
However, the etching of the aluminum was stronger than expected resulting in an over-etching of $6.7\mu m$ rather than the anticipated $0.5\mu m$. This over-etching is shown in figure 5.2.

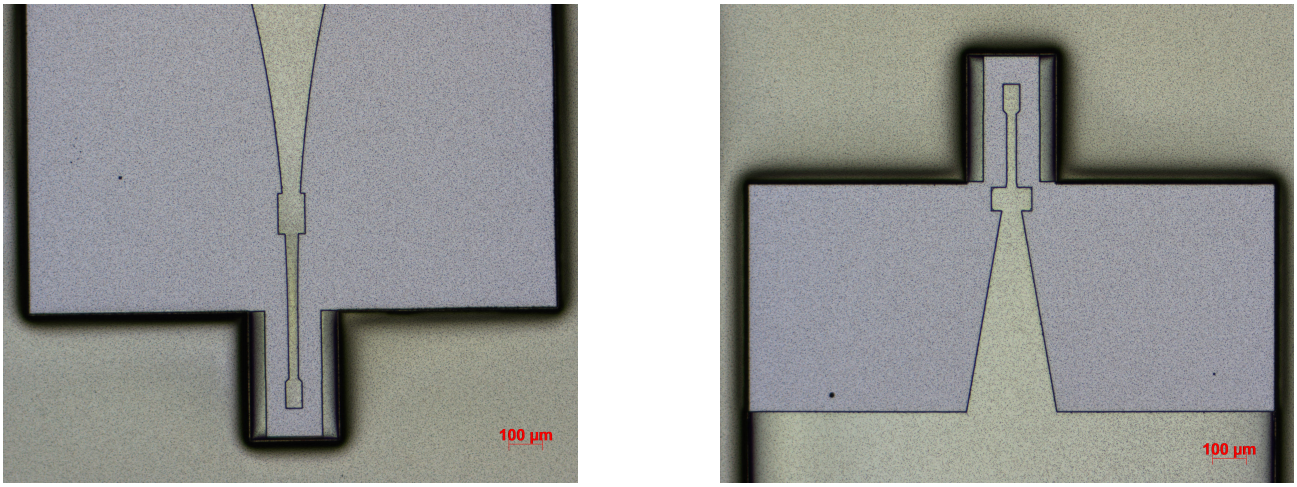

(a) Final elliptic transition

(b) Final tapered transition

Figure 5.1: Fabricated transitions

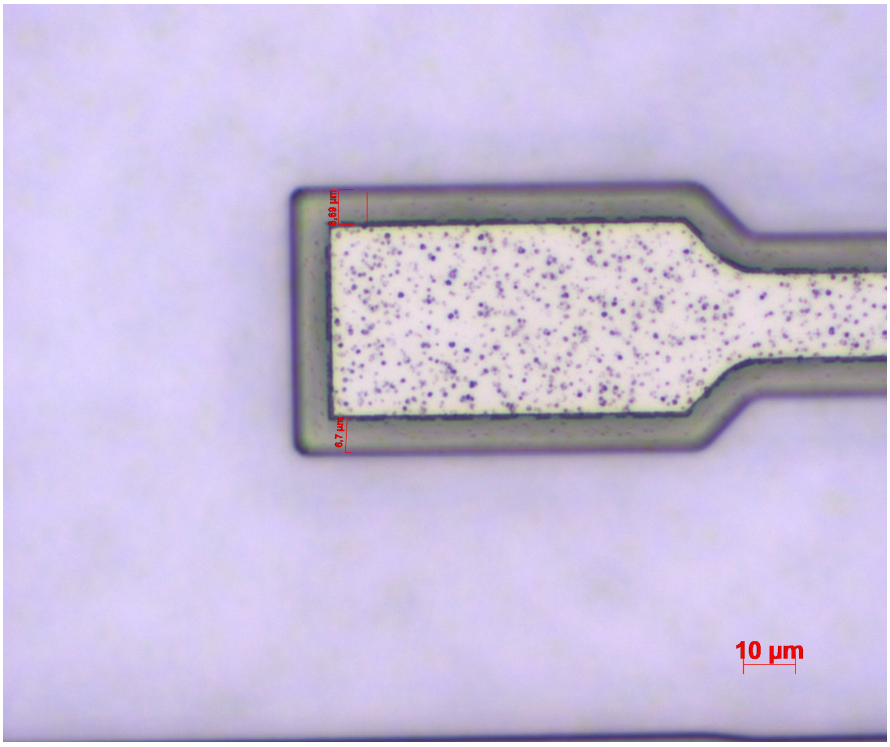

Figure 5.2: Over-etching of $7\mu m$

The over-etching of $6.7\mu m$ represents a big problem on two levels.
Firstly, in terms of measurements, placing the probes on the GCPW pads will be complicated since their central tracks are now $13.4\mu m$ smaller and the gaps are now $13.4\mu m$ bigger than the dimensions needed for good measurements.

Secondly, the characteristics of the structures change completely. Indeed, a thinner width means a higher impedance for the GCPW lines and a less good matching for the transitions. To illustrate this point, figure 5.3 shows the calibrated impedance of fabricated GCPW lines. The characteristic impedance is approximately equal to 80Ω instead of the designed 50Ω.

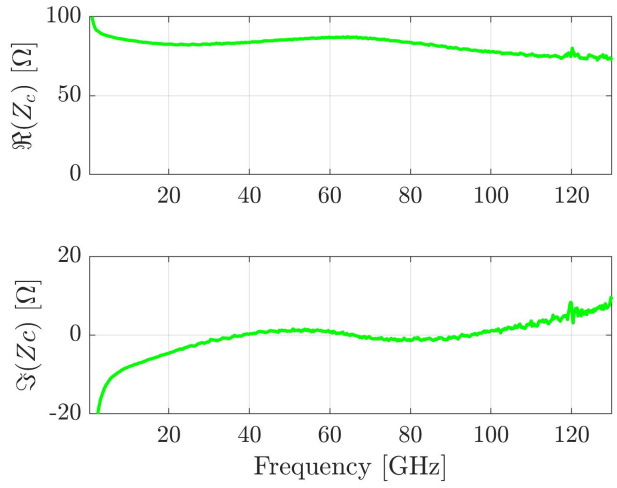

Figure 5.3: Calibrated impedance of a fabricated GCPW line with over-ethcing

Another problem with manufacturing is that the metal pulls out of the structure after the probes are placed for measurement. This is probably due to the metal still being too soft after fabrication.
This problem complicates measurements because if a measurement gives inconsistent results, it is more difficult to make that measurement again. Figure 5.4 shows the pads after measurement as an illustration. It can also be seen on this figure that to make a new measurement, the probe had to be moved.

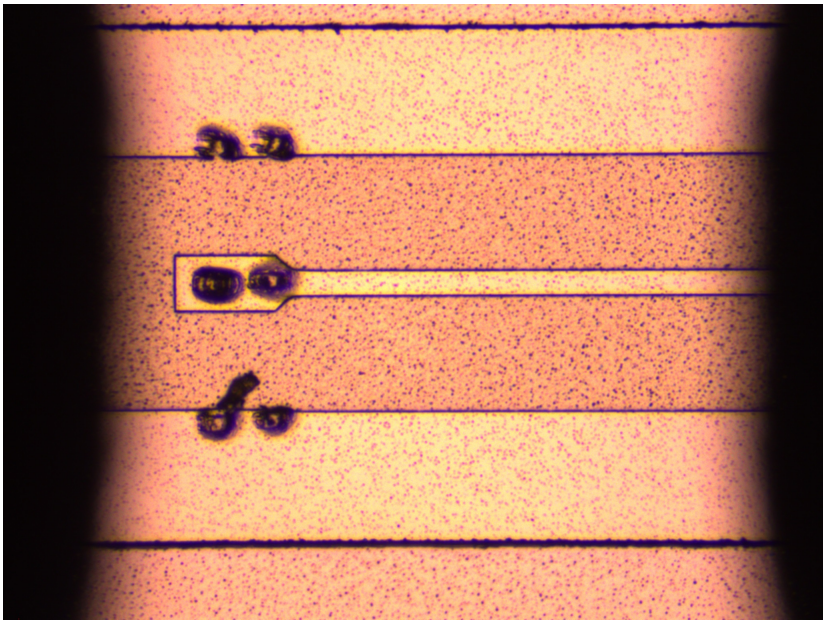

Figure 5.4: Pulling out of metal after measurement

5.2 Results

The measurements are made using the *Prober MPI 300mm* probe station of the Welcome lab located in Louvain-La-Neuve.

In order to have more chances to have correct measurements, these are made on two different matrices which seem to be the best manufactured. In addition, they are made on the structures anticipating the theoretical over-etching of $1.5\mu m$ in order to minimize the effect of the real over-etching.
The following presents the de-embedded performance of the transitions.
Only the results for the best of the two dies are presented so as not to make the reading too heavy.

5.2.1 De-embedded results

The first step in order to de-embed the results is to apply the mTRL on the GCPW lines.
To find out if the calibration is successful, the estimate of the propagation constant is shown in figure 5.5. If the mTRL algorithm is successful, this estimation is relatively constant, which is the case here. The effet of the GCPW section may thus be removed from the final results.

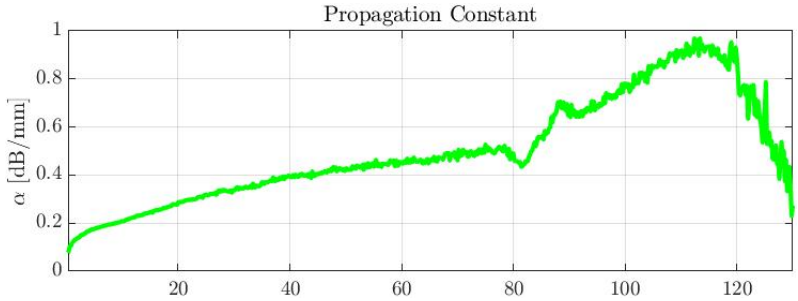

Figure 5.5: Estimation of the propagation constant of the GCPW lines

The same manipulation is performed for the back-to-back configuration of the final tapered transition and the the back-to-back configuration of the final elliptic transition. Figure 5.6 and 5.7 show the results, respectively.
Unfortunately, due to manufacturing problems, the estimates are not really good, especially for the final tapered transition. This means that the effects of the SIW sections of the back-to-back configurations will be poorly removed when doing the de-embedding.
In spite of this, the de-embedded S_{11} scattering parameters are shown respectively in figures 5.8 and 5.9.

A good point of these results is that they have the same behaviors, with a frequency shift, as those presented in section 3.3, even though the performance is not the same in absolute terms. With return loss higher than $5dB$, the elliptic transition even has good results considering the context.

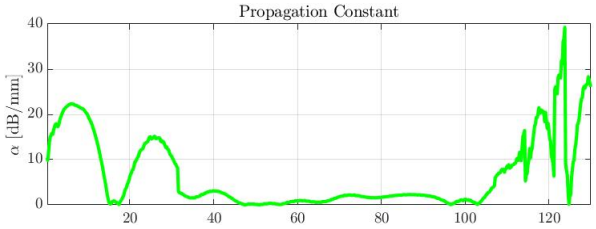

Figure 5.6: Estimation of the propagation constant of the back-to-back configuration of the final tapered transition

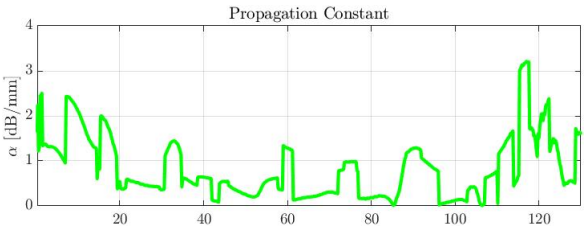

Figure 5.7: Estimation of the propagation constant of the back-to-back configuration of the final elliptic transition

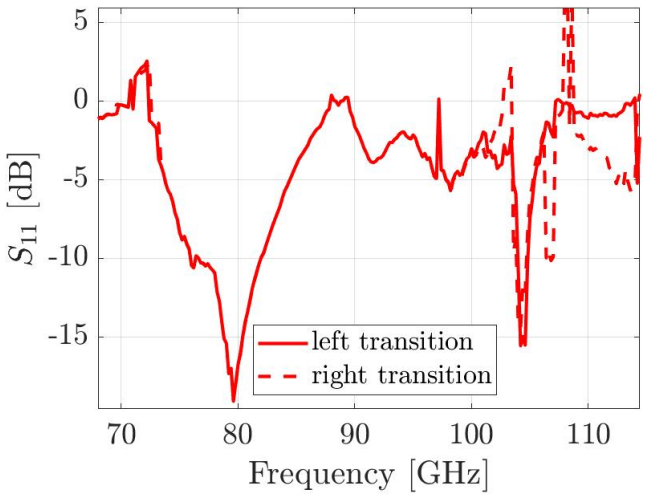

Figure 5.8: De-embedded S_{11} scattering parameter from the measurements of the final tapered transition in dB scale

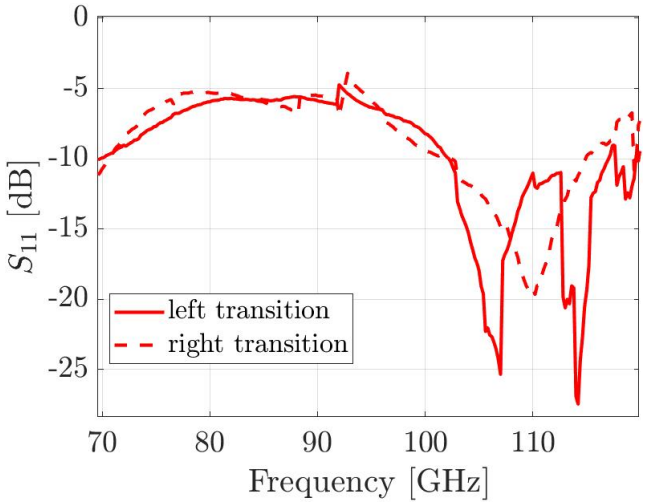

Figure 5.9: De-embedded S_{11} scattering parameter from the measurements of the final elliptic transition in dB scale

5.3 Discussion

The relatively poor results presented above are not so surprising considering the various problems related to manufacturing. Indeed, as already mentioned, the over-etching is such that the transitions are no longer matched in the way they were designed.
However, the fact that the insertion losses have the same trend as those resulting from the simulations is encouraging.
Due to lack of time and resources, a new fabrication of transitions could not be performed for this work.

Chapter 6

Conclusion

As a conclusion, a summary to highlight the contribution of this master's thesis and the description of further research directions in the framework of this work are done.

6.1 Contribution of this work

The study of the literature showed a real interest in designing grounded coplanar waveguide to substrate-integrated waveguide transitions for the W-band. Indeed, there are few transitions for this band.
In this master's thesis, two new GCPW to SIW transitions were designed.
The first one is called "Tapered transition with discontinuous element and without side grounds". It achieves a return loss higher than $10dB$ and a return loss lower than $0.8dB$ over 88% of the W band in simulations.
The second one is called "elliptic transition with discontinuous element". It achieves a return loss higher than $9dB$ with a peak at $30dB$ and a return loss lower than $1.1dB$ over the entire W band in simulations.
In addition to the design of transitions, a design of a mask to fabricate the transitions to be able to measure them using a mTRL calibration was done. This mask was also designed to prevent for a normal over-etching.
Finally, tests of the manufactured transitions were performed. Unfortunately, due to manufacturing problems, the results were not satisfying but they allowed to show that the general shape of the simulation performance is well reflected in the measured performance.

6.2 Further research direction

Four further research directions can be identified.

- Since a simulation problem was found late in the design process of the transitions of chapter 2, a new optimization of the designed transitions would be convenient.
- A sensitivity analysis of the designed transition could also be performed.
- As it was mentioned in section 5.3, a new manufacturing of the transitions was not possible in the framework of this work. This could be a good starting point for a following work.

- Since this work is about design, fabrication and testing, the transitions were not used for actual applications. Yet, it could be a great research subject.

Bibliography

[1] D. Deslandes and K. Wu. Integrated microstrip and rectangular waveguide in planar form. *IEEE Microwave and Wireless Components Letters*, 11(2):68–70, 2001.

[2] G. Acri, E. Pistono, F. Podevin, P. Ferrari, L. Boccia, A. S. Grimault-Jacquin, N. Zerounian, F. Aniel, and L. Vincent. BenzoCycloButene-based in-Package Substrate Integrated Waveguides for sub-THz Applications. In *2020 50th European Microwave Conference, EuMC 2020*, pages 41–44. Institute of Electrical and Electronics Engineers Inc., 1 2021.

[3] Te Yen Chiu and Chun Hsing Li. Low-Loss Low-Cost Substrate-Integrated Waveguide and Filter in GaAs IPD Technology for Terahertz Applications. *IEEE Access*, 9:86346–86357, 2021.

[4] Dominic Deslandes and Ke Wu. Design consideration and performance analysis of substrate integrated waveguide components. In *2002 32nd European Microwave Conference*, pages 1–4, 2002.

[5] D.M. Pozar. *Microwave Engineering, 4th Edition*. Wiley, 2011.

[6] J Coonrod and B Rautio. Comparing microstrip and cpw performance. 55:74–+, 2012.

[7] Rainee N Simons. *Coplanar waveguide circuits, components, and systems*. John Wiley & Sons, 2004.

[8] Beere R S, Am Khan, and Manjunatha Reddy. Global journal of trends in engineering simulation study on insertion and return loss of planar transmission lines for different dielectric substrates. 04 2015.

[9] Dominic Deslandes. Design equations for tapered microstrip-to-substrate integrated waveguide transitions. In *2010 IEEE MTT-S International Microwave Symposium*, pages 704–707, 2010.

[10] Federal communications commission. LMDS Band Allocation (Local Multipoint Distribution Service). Technical report, Federal communications commission.

[11] Zamzam Kordiboroujeni and Jens Bornemann. New wideband transition from microstrip line to substrate integrated waveguide. *IEEE Transactions on Microwave Theory and Techniques*, 62(12):2983–2989, 12 2014.

[12] Hector Esteban, Angel Belenguer, Juan R. Sanchez, Carmen Bachiller, and Vicente E. Boria. Improved Low Reflection Transition from Microstrip Line to Empty Substrate-Integrated Waveguide. *IEEE Microwave and Wireless Components Letters*, 27(8):685–687, 8 2017.

[13] Alfonso Gomez Garcia, Yolanda Campos-Roca, Rafael Gomez Alcala, and Jesus Rubio. Multistep Transitions from Microstrip and GCPW Lines to SIW in 5G 26 GHz Band. *IEEE Access*, 9:68778–68787, 2021.

[14] Dong Sik Eom and Hai Young Lee. Substrate integrated waveguide transitions to planar transmission lines using lumped elements and their applications. *IEEE Transactions on Microwave Theory and Techniques*, 64(12):4352–4361, 12 2016.

[15] D. Deslandes and Ke Wu. Integrated transition of coplanar to rectangular waveguides. In *2001 IEEE MTT-S International Microwave Sympsoium Digest (Cat. No.01CH37157)*, volume 2, pages 619–622 vol.2, 2001.

[16] Andreas Patrovsky, Maxime Daigle, and Ke Wu. Millimeter-wave wideband transition from cpw to substrate integrated waveguide on electrically thick high-permittivity substrates. In *2007 European Microwave Conference*, pages 138–141, 2007.

[17] Farzaneh Taringou, Jens Bornemann, and Ke Wu. Experimental verification of coplanar-to-substrate-integrated-waveguide interconnect on low-permittivity substrate. In *2013 Asia-Pacific Microwave Conference Proceedings (APMC)*, pages 104–106, 2013.

[18] Sunho Lee, Sangwoon Jung, and Hai Young Lee. Ultra-wideband CPW-to-substrate integrated waveguide transition using an elevated-CPW section. *IEEE Microwave and Wireless Components Letters*, 18(11):746–748, 11 2008.

[19] Robab Kazemi, Aly E. Fathy, Songnan Yang, and R. Ali Sadeghzadeh. Development of an ultra wide band GCPW to SIW transition. In *RWW 2012 - Proceedings: IEEE Radio and Wireless Symposium, RWS 2012*, pages 171–174, 2012.

[20] R Levy. A Generalized Design Technique for Practical Distributed Reciprocal Ladder Networks. *IEEE Transactions on Microwave Theory and Techniques*, 21(8):519–526, 1973.

[21] Xiao-Ping Chen and Ke Wu. Low-loss ultra-wideband transition between conductor-backed coplanar waveguide and substrate integrated waveguide. In *IEEE MTT-S International Microwave Symposium Digest*, pages 349–352, 2009.

[22] Dominic Deslandes and Ke Wu. Analysis and design of current probe transition from grounded coplanar to substrate integrated rectangular waveguides. *IEEE Transactions on Microwave Theory and Techniques*, 53(8):2487–2494, 2005.

[23] Yujian Li and Kwai Man Luk. A broadband V-band rectangular waveguide to substrate integrated waveguide transition. *IEEE Microwave and Wireless Components Letters*, 24(9):590–592, 9 2014.

[24] J. Li, G. Wen, and F. Xiao. Broadband transition between rectangular waveguide and substrate integrated waveguide. *Electronics Letters*, 46(3):218–219, 2010.

[25] Soumava Mukherjee, Prasun Chongder, Kumar Vaibhav Srivastava, and Animesh Biswas. Design of a broadband coaxial to substrate integrated waveguide (siw) transition. In *2013 Asia-Pacific Microwave Conference Proceedings (APMC)*, pages 896–898, 2013.

[26] Farzaneh Taringou, Thomas Weiland, and Jens Bornemann. Broadband design of substrate integrated waveguide to stripline interconnect. In *2014 International Conference on Numerical Electromagnetic Modeling and Optimization for RF, Microwave, and Terahertz Applications (NEMO)*, pages 1–4, 2014.

[27] Processing procedures for cyclotene 3000 series dry etch resins, 2005.

[28] D M Pozar. *Microwave Engineering, 4th Edition*, pages 110–121. Wiley, 2011.

[29] Michael Steer. 6.4: Rectangular waveguide, May 2022.

[30] D M Pozar. *Microwave Engineering, 4th Edition*, pages 422–426. Wiley, 2011.

[31] R.B. Marks and D.F. Williams. Characteristic impedance determination using propagation constant measurement. *IEEE Microwave and Guided Wave Letters*, 1(6):141–143, 1991.

[32] R.B. Marks. A multiline method of network analyzer calibration. *IEEE Transactions on Microwave Theory and Techniques*, 39(7):1205–1215, 1991.

[33] Roger B. Marks. Formulations of the basic vector network analyzer error model including switch-terms. In *50th ARFTG Conference Digest*, volume 32, pages 115–126, 1997.

[34] D.C. DeGroot, J.A. Jargon, and R.B. Marks. Multiline trl revealed. In *60th ARFTG Conference Digest, Fall 2002.*, pages 131–155, 2002.

UNIVERSITÉ CATHOLIQUE DE LOUVAIN
École polytechnique de Louvain
Rue Archimède, 1 bte L6.11.01, 1348 Louvain-la-Neuve, Belgique | **www.uclouvain.be/epl**